NUMERICAL STUDY OF CAVITATION WITHIN ORIFICE FLOW

A Thesis

by

PENGZE YANG

Submitted to the Office of Graduate and Professional Studies of
Texas A&M University
in partial fulfillment of the requirements for the degree of

MASTER OF SCIENCE

Chair of Committee,	Robert Handler
Committee Members,	David Staack
	Prabir Daripa
Head of Department,	Andreas Polycarpou

December 2015

Major Subject: Mechanical Engineering

ABSTRACT

Cavitation generally occurs when the pressure at certain location drops to the vapor pressure and the liquid water evaporates as a consequence. For the past several decades, numerous experimental researches have been conducted to investigate this phenomenon due to its degradation effects on hydraulic device structures, such as erosion, noise and vibration. A plate orifice is an important restriction device that is widely used in many industries. It serves functions as restricting flow and measuring flow rate within a pipe. The plate orifice is also subject to intense cavitation at high pressure difference, therefore, the simulation research of the cavitation phenomenon within an orifice flow becomes quite essential for understanding the causes of cavitation and searching for possible preventing methods. In this paper, all researches are simulation-oriented by using ANSYS FLUENT due to its high resolution comparing to experiments. Standard orifice plates based on ASME PTC 19.5-2004 are chosen and modeled in the study with the diameter ratio from 0.2 to 0.75. Steady state studies are conducted for each diameter ratio at the cavitation number roughly from 0.2 to 2.5 to investigate the dependency of discharge coefficient on the cavitation number. Meanwhile, a study of the flow regime transition due to cavitation is also carried out based on the steady state results. Moreover, a transient study is done to clarify the relationship between cavitation at the orifice and cavitation at the downstream pipe wall. Several conclusions can be made from this numerical study. The discharge coefficient of the orifice plate is independent of cavitation number; As cavitation number decreases, cavitation tends to be more intense and the flow regime transit to super cavitation eventually; In addition to cavitation occurring at the orifice edge, it also initiates at downstream pipe wall.

TABLE OF CONTENTS

Page

Page

LIST OF FIGURES

Page

Page

LIST OF TABLES

Page

CHAPTER I

INTRODUCTION

In many engineering applications, especially high-pressure devices, cavitation has been the subject of extensive theoretical and experimental research since it has predominantly been perceived as an undesirable phenomenon. This is mainly due to the detrimental effects of cavitation such as erosion, noise and vibration, caused by the growth and collapse of vapor bubbles. In the liquid flow, cavitation generally occurs if the pressure in a certain location drops below the vapor pressure and consequently the negative pressure is relieved by the formation of gas-filled or gas and vapor-filled cavities. Cavitation occurs by the sudden expansion and the volumetric oscillation of bubble nuclei in the water due to ambient pressure changes. Knapp et al [1] reported that cavitation can be classified into several different regimes: traveling, fixed and vortex cavitation. Cavitating flows often lead to performance degradation and structural damage to many hydraulic devices. These effects are related to the size, the time averaged shapes of the vaporized structures, and their area of influence. Pumps, valves, propellers, nozzles and numerous other devices can be affected by cavitation. For several years, numerous researchers have obtained experimental data about the cavitation inception and development for flow elements such as nozzles, orifices, venturies (Nurick [2], Abuaf et al. [3], Meyer et al. [4] and Stutz and Reboud [5]).

Mechanical degradation of a solid material caused by cavitation is called cavitation erosion. Cavitation erosion can be formed when the cavity implosions are violent enough and they take place near enough to the solid material. Cavitation erosion can be identified from a specific rough mark in the surfaces of the component flow paths. Despite the great deal of research on this phenomenon, the actual mechanism of cavitation erosion is still not fully clear. At present it is considered that there are two possible mechanisms to cause cavitation erosion. When a cavity collapses within the body of liquid, the collapse is symmetrical. The symmetrical collapse of a cavity emits a shock wave to the surrounding liquid (see Figure 1). When a cavity is in contact with or very close to the solid boundary,

the collapse is asymmetrical. In asymmetrical collapse the cavity is perturbed from the side away from the solid boundary and finally the fluid is penetrating through the cavity and a micro-jet is formed (see Figure 1). However, it has been stated (Hansson and Hansson [6], Preece [7]) that each of these mechanisms has features that do not give a full explanation of the observed cavitation erosion phenomena. The shock wave is attenuated too rapidly and the radius of the cavity micro-jet is too small to produce the degree of overall cavitation erosion observed in experiments. Nevertheless, when a cloud of cavities collapses, the cavities do not act independently, but enhances the effects of each other.

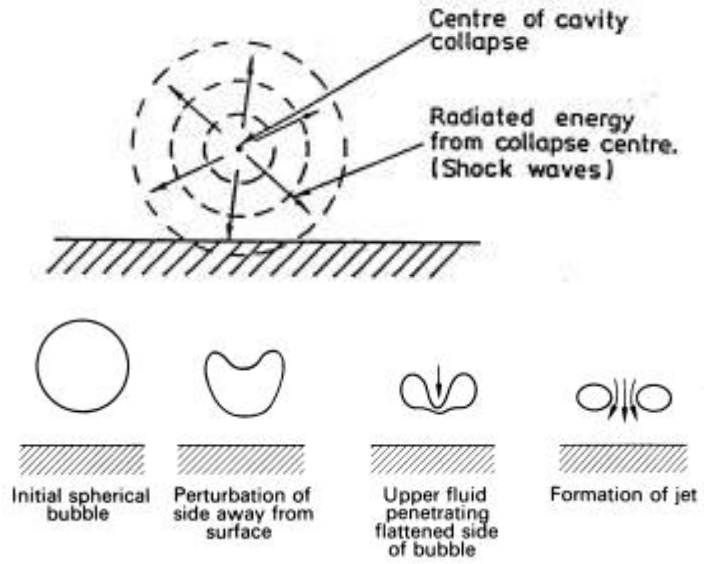

Figure 1 The shock-wave mechanism and the micro-jet mechanism of the cavitation erosion. (Lamb [8], Knapp et al. [1])

In many industrial plants like oil and gas refineries, power generation plants or chemical plants, oil transport pipelines, restriction orifices such as the single-hole orifice, the multi-perforated orifice, and the cone type orifice are widely used to restrict the flow and measure the flow rate within many such systems.

Figure 2 below shows different types of orifices. When the pressure difference between two sides of an orifice is high, cavitation is likely. Since the severity of damage caused by cavitation is well known, research has to be done to investigate the reason causing this devastating phenomenon and come up with possible methods to eliminate it as much as possible. For the past few decades, numerous researchers have put significant effort into solving these problems caused by cavitation. For example, J.F Bailey [9] and G. Ruppel [10] both conducted experiments on cavitation within orifice plate. The former investigated the effects of water temperature on cavitation, while the latter explored the effects of flow rate. F. Numachi and M. Yamabe [11] also did research on cavitation in orifice flow. They focused their research on cavitation effects on the discharge coefficient of a sharp-edged orifice plate. They found that for a given diameter ratio, the discharge coefficient is independent of cavitation number and that the inception cavitation number is independent of the diameter ratio. B.C. Kim, B.C.Pak [12] did similar experiments but focused more on the orifice plates with small diameter ratios. In their experiments, the effects of cavitation and plate thickness for small diameter ratio orifice plates were evaluated in a 100 mm diameter test section of a water flow calibration facility.

Numerical simulation of cavitation in an orifice has also been undertaken by several researchers. However, these simulations are mainly about cavitation in the large aspect ratio orifice plates. S.Dairi and D. D. Joseph [13] were trying to identify the potential locations for cavitation induced by the total stress on the flow of a liquid through an orifice with length to diameter ratio between 1 and 5. Similarly, Xu [14] investigated the effects of various parameters on an orifice internal cavitating flow with length to diameter ratio of 3~5. His study focused on the unsteadiness caused by the hydrodynamic instability of the vena-contracta or the presence of cavitation in this region.

In all, very few numerical studies have been done in terms of cavitation in the standard orifice plate.

Therefore, in this paper, research will be focused on cavitating flow within an ASME standard [15] orifice plate with diameter ratio from 0.2 to 0.75, using ANSYS FLUENT.

The effects of cavitation on the discharge coefficient will be studied and results will be compared to experiments. Potential cavitation regions will also be located in the flow domain and the reasons leading the cavitation will be determined.

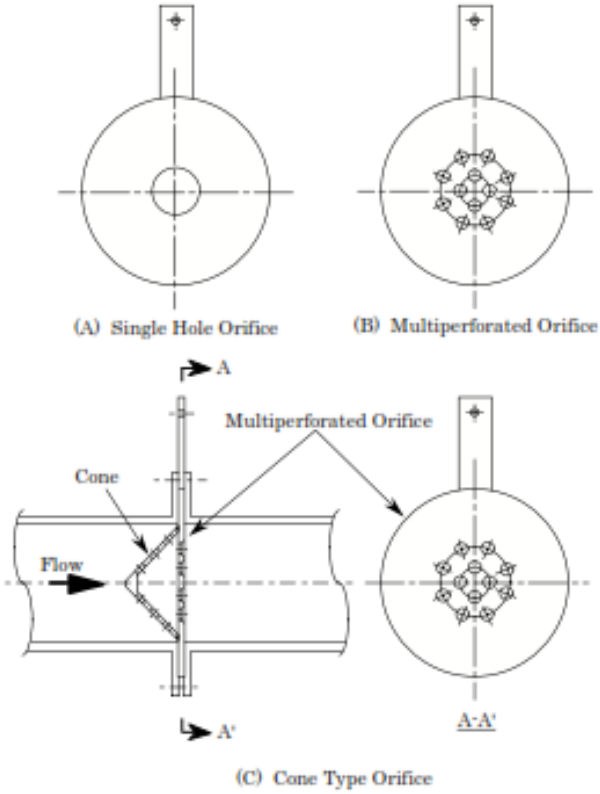

Figure 2 Restriction orifices. (Takahashi, Matsuda and Miyamoto, 2001)

The specifications for conventional orifice plates are described in both ISO 5167 and ASME PTC 19.5 [16]. A schematic of standard orifice plate placed in a pipe is shown in Figure 3 below. The minimum throat diameters recommended by ISO 5167 and ASME Report are 12.5 and 11.4 mm, respectively. Normally, a 45° bevel is specified for the downstream face of the plate with a throat edge thickness and plate thickness**.** In ASME PTC, the throat edge thickness, e, is 0.02 > e/D >0.005 while the plate thickness, E, is e <

E < 0.05 D. In this paper, orifice plates with 6 different diameter ratio are chosen with plate thickness 3.2mm and edge thickness 1.6mm. The specifications for these orifice plates are listed in Table 1 below.

Table 1 Specification for orifice plates

beta	Pipe diameter (mm)	Orifice diameter (mm)	Plate thickness (mm)	Length to diameter ratio
0.2	100	20	3.2	0.16
0.3	100	30	3.2	0.107
0.4	100	40	3.2	0.08
0.5	100	50	3.2	0.064
0.6	100	60	3.2	0.053
0.75	100	75	3.2	0.043

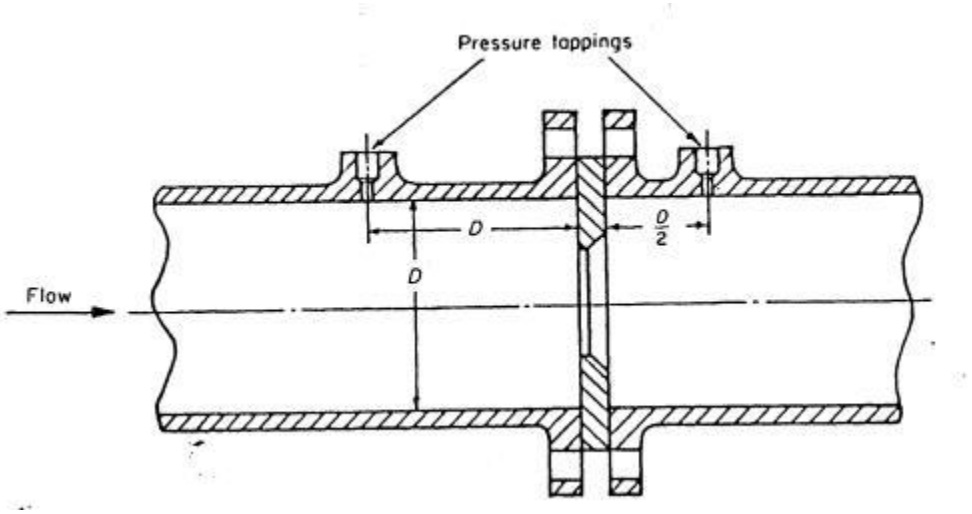

Figure 3 ASME standard sharp edge orifice with D and D/2 pressure tapping [16].

CHAPTER II

OBJECTIVES

(1). A steady state study of the effects of cavitation on the discharge coefficient will be conducted and the results will be compared to experiments done by Numachi [11]. By 'steady state' we mean that all computed flow parameters are averages, and therefore independent of time. More specifically, several ASME standard orifice plates with different diameter ratio mentioned in the previous section, will be modeled in FLUENT. For each diameter ratio, the orifice cavitation numbers are obtained at steady state by altering the pressure difference between pipe inlet and outlet. The dependence of the discharge coefficient on cavitation number will be determined for each orifice plate diameter ratio. This result will be compared to that of Numachi.

(2). Y. Yan and R. B. Thorpe [17] presents both experimental and theoretical aspects of the flow regime transitions caused by cavitation when water is passing through an orifice. Within their experiments, cavitation inception marks the transition from single-phase to two-phase bubbly flow; choked cavitation marks the transition from two-phase bubbly flow to two-phase annular jet flow. We will compare our computational results to these experimental results concerning the effects of cavitation on the flow regime transition. In our numerical study, a specific orifice diameter ratio will be chosen for this task. The volume fraction of vapor within the whole flow field will be presented at different cavitation numbers, which can give us some clues concerning the dependence of the flow regime on the presence of cavitation.

(3). A transient study of cavitation inception and growth will be carried out for a specific orifice plate model at a specific pressure difference. This study will highlight the dynamic features associated with cavitation in this geometry. The simulation will cover the time ranging from 0s to 0.21s with 0.01s increment. Snapshots of vapor volume fraction distribution will be obtained at every time instance to elucidate the inception and growth of cavitation.

CHAPTER III

APPROACH

III.1 Theoretical Models

Our computational model is based on the following equations expressing conservation of mass, and momentum in a two phase system, along with a cavitation model.

Continuity Equation $$\frac{\partial \rho_m}{\partial t} + \vec{\nabla} \bullet (\rho_m \vec{V}) = 0$$

Conservation of Momentum $$\frac{\partial(\rho_{\mathrm{m}} V_i)}{\partial t} + \frac{\partial(\rho_{\mathrm{m}} V_i V_j)}{\partial x_j} = -\frac{\partial P}{\partial x_i} + \frac{1}{3}\mu \frac{\partial V_j}{\partial x_j} + \mu\left(\frac{\partial^2 V_i}{\partial x_j \partial x_j}\right)$$

Cavitation Model $$\frac{\partial \alpha_v \rho_v}{\delta t} + \frac{\partial \alpha_v \rho_v V_j}{\delta x_j} = \Delta R$$

Where, ρ_v is vapor density; α_v represents vapor volume fraction; ρ_m is mixture density, which can be expressed as $\rho_m = \alpha_v \rho_v + (1-\alpha_v)\rho_l$; ρ_l is water liquid density.

Derivation of governing equations of cavitation flow is presented below.

III.1.1 Continuity Equation

In order to derive the continuity equation, control volume method is used to better illustrate relationship between net mass flux rate and mass change rate within the CV.

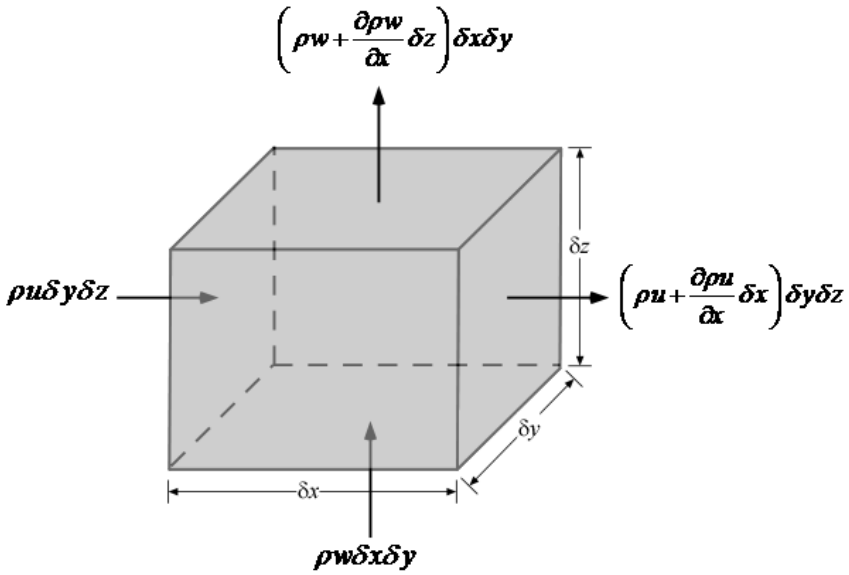

Figure 4 CV for continuity equation

Net mass flux of the CV is,

$$-(\frac{\partial \rho_m u}{\partial x} + \frac{\partial \rho_m v}{\partial y} + \frac{\partial \rho_m w}{\partial z})\delta x\delta y\delta z$$

Mass change rate within CV can be expressed as,

$$\frac{\partial \rho_m V}{\partial t} \text{ , where } V = \delta x\delta y\delta z$$

Therefore,

$$-(\frac{\partial \rho_m u}{\partial x} + \frac{\partial \rho_m v}{\partial y} + \frac{\partial \rho_m w}{\partial z})\delta x\delta y\delta z = \frac{\partial \rho_m}{\partial t}\delta x\delta y\delta z$$

$$\frac{\partial \rho_m}{\partial t} + \frac{\partial \rho_m u}{\partial x} + \frac{\partial \rho_m v}{\partial y} + \frac{\partial \rho_m w}{\partial z} = 0$$

III.1.2 Conservation of Momentum

Like above, control volume method is used to explain how momentum change rate within the CV corresponds to net stress on CV's surfaces, based on Newton's Second Law $\vec{F} = \frac{d\vec{P}}{dt}$.

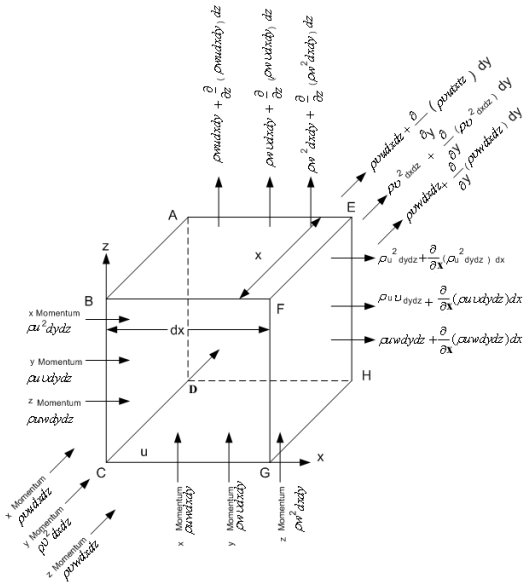

Figure 5 CV for net momentum flux analysis

Take y direction for example,

Net influx of momentum in y direction due to mass influx:

$$(\frac{\partial \rho_m vv}{\partial y} + \frac{\partial \rho_m uv}{\partial x} + \frac{\partial \rho_m wv}{\partial z})\delta x \delta y \delta z$$

Net accumulation rate is

$$\frac{\partial \rho_m v}{\partial t}\delta x \delta y \delta z$$

So the momentum change rate within CV on y direction can be expressed as:

$$(\frac{\partial \rho_m vv}{\partial y}+\frac{\partial \rho_m uv}{\partial x}+\frac{\partial \rho_m wv}{\partial z})\delta x\delta y\delta z+\frac{\partial \rho_m v}{\partial t}\delta x\delta y\delta z$$

While on the other hand, stress on CV's surfaces in term of y direction can be shown as below (suppose index 1 represents y direction)

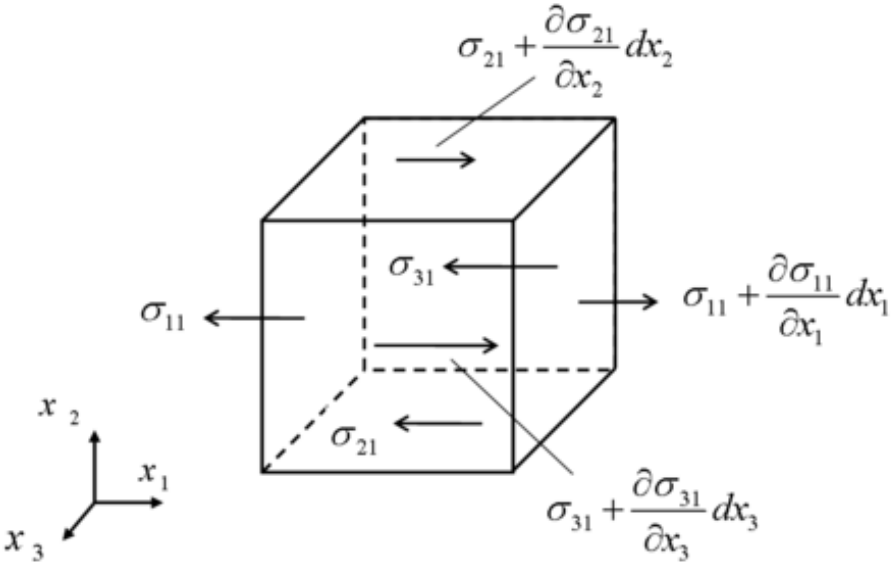

Figure 6 CV for net stress analysis

Based on the CV analysis, three couples of stress act on y direction, either on positive or negative. So net stress applied on y direction is,

$$(\frac{\partial \sigma_{yy}}{\partial y}+\frac{\partial \tau_{zy}}{\partial z}+\frac{\partial \tau_{xy}}{\partial x})\delta x\delta y\delta z$$

Therefore, based on Newton's Second Law,

$$\frac{\partial \rho_m v}{\partial t}+\frac{\partial \rho_m vv}{\partial y}+\frac{\partial \rho_m uv}{\partial x}+\frac{\partial \rho_m wv}{\partial z}=\frac{\partial \sigma_{yy}}{\partial y}+\frac{\partial \tau_{zy}}{\partial z}+\frac{\partial \tau_{xy}}{\partial x}$$

Given the Stokes Constitutive Equation

$$\tau_{ij}=(-P-\frac{2}{3}\mu\vec{\nabla}\bullet\vec{V})\delta_{ij}+\mu(\frac{\partial u_i}{\partial x_j}+\frac{\partial u_j}{\partial x_i})$$

Where $\delta_{ij}=1 \quad for\ i=j$
$\delta_{ij}=0 \quad for\ i\neq j$

If substitute the stresses in COM with Stokes Constitutive Equation, yields,

$$\frac{\partial \rho_m v}{\partial t}+\frac{\partial \rho_m vv}{\partial y}+\frac{\partial \rho_m uv}{\partial x}+\frac{\partial \rho_m wv}{\partial z}=-\frac{\partial P}{\partial y}+\frac{1}{3}\mu(\frac{\partial u}{\partial x}+\frac{\partial v}{\partial y}+\frac{\partial w}{\partial z})+\mu(\frac{\partial^2 v}{\partial x^2}+\frac{\partial^2 v}{\partial y^2}+\frac{\partial^2 v}{\partial z^2})$$

Similarly, conservation of momentum in all directions can be expressed as,

$$\frac{\partial \rho_m u}{\partial t}+\frac{\partial \rho_m vu}{\partial y}+\frac{\partial \rho_m uu}{\partial x}+\frac{\partial \rho_m wu}{\partial z}=-\frac{\partial P}{\partial x}+\frac{1}{3}\mu(\frac{\partial u}{\partial x}+\frac{\partial v}{\partial y}+\frac{\partial w}{\partial z})+\mu(\frac{\partial^2 u}{\partial x^2}+\frac{\partial^2 u}{\partial y^2}+\frac{\partial^2 u}{\partial z^2})$$

$$\frac{\partial \rho_m v}{\partial t}+\frac{\partial \rho_m vv}{\partial y}+\frac{\partial \rho_m uv}{\partial x}+\frac{\partial \rho_m wv}{\partial z}=-\frac{\partial P}{\partial y}+\frac{1}{3}\mu(\frac{\partial u}{\partial x}+\frac{\partial v}{\partial y}+\frac{\partial w}{\partial z})+\mu(\frac{\partial^2 v}{\partial x^2}+\frac{\partial^2 v}{\partial y^2}+\frac{\partial^2 v}{\partial z^2})$$

$$\frac{\partial \rho_m w}{\partial t}+\frac{\partial \rho_m vw}{\partial y}+\frac{\partial \rho_m uw}{\partial x}+\frac{\partial \rho_m ww}{\partial z}=-\frac{\partial P}{\partial z}+\frac{1}{3}\mu(\frac{\partial u}{\partial x}+\frac{\partial v}{\partial y}+\frac{\partial w}{\partial z})+\mu(\frac{\partial^2 w}{\partial x^2}+\frac{\partial^2 w}{\partial y^2}+\frac{\partial^2 w}{\partial z^2})$$

III.1.3 Cavitation Model

Similar to continuity equation, cavitation model is also a mass conservation equation which is able to be derived by control volume method. The main difference is cavitation model focuses on mass conservation equation with respect to water vapor. Another thing worth pointing out is cavitation model also contains source and sink terms of water vapor governed by Rayleigh-Plesset Equation.

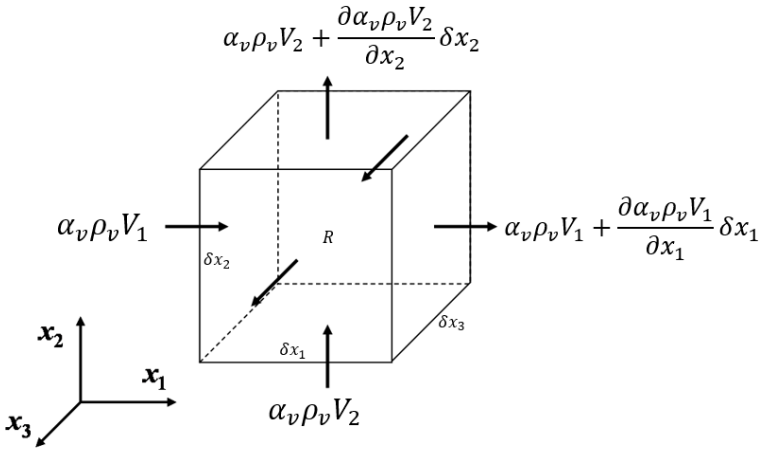

Figure 7 CV for vapor transport equation

Therefore, cavitation model (also known as Vapor Transport Equation) is

$$\frac{\partial \alpha_v \rho_v}{\partial t} + \frac{\partial \alpha_v \rho_v V_j}{\partial x_j} = \Delta R$$

Where, ΔR is the source (or sink) term of water vapor.

III.2 Fluent Adapted Momentum and Cavitation Model

At the Reynold's number that we anticipate, the flow will be fully turbulent in all cases. Therefore, we will use a turbulence model to solve for the time-averaged flow. We have chosen to use the realizable k-epsilon model [17]. At the same time, the Schnerr-Sauer model [17] is applied for the cavitation model. The details of these models are given below.

III.2.1 k-epsilon Model

By applying the k-epsilon model, the velocity and pressure term in the continuity and moment equations are decomposed into a mean component and a fluctuation component. Afterwards, the Reynolds average Navier-Stokes transformation is carried out for the governing equations. As a result, the k and epsilon transport equation in k-epsilon realizable model can be expressed as below,

$$\frac{\partial}{\partial t}(\rho k)+\frac{\partial}{\partial x_j}(\rho k u_j)=\frac{\partial}{\partial x_j}\left[\left(\mu+\frac{\mu_t}{\sigma_k}\right)\frac{\partial k}{\partial x_j}\right]+P_k+P_b-\rho\epsilon-Y_M+S_k$$

$$\frac{\partial}{\partial t}(\rho\epsilon)+\frac{\partial}{\partial x_j}(\rho\epsilon u_j)=\frac{\partial}{\partial x_j}\left[\left(\mu+\frac{\mu_t}{\sigma_\epsilon}\right)\frac{\partial \epsilon}{\partial x_j}\right]+\rho C_1 S\epsilon-\rho C_2\frac{\epsilon^2}{k+\sqrt{\nu\epsilon}}+C_{1\epsilon}\frac{\epsilon}{k}C_{3\epsilon}P_b+S_\epsilon$$

Where,

$$C_1=\max\left[0.43,\frac{\eta}{\eta+5}\right],\qquad \eta=S\frac{k}{\epsilon},\qquad S=\sqrt{2S_{ij}S_{ij}}$$

Constants are, $C_{1\epsilon}=1.44,\ \ C_2=1.9,\ \ \sigma_k=1.0,\ \ \sigma_\epsilon=1.2$

Within the equations above, P_k represents the generation of turbulence kinetic energy due to the mean velocity gradients. P_b is the generation of turbulence kinetic energy due to buoyancy, in this case, equate to zero. Y_m represents the contribution of the fluctuating dilatation in compressible turbulence to the overall dissipation rate, which is also zero in this case. The same happens to S_k and S_e which are the user defined source.

III.2.2 Schnerr-Sauer Model

The Schnerr-Sauer model is implemented in all cavitation simulations. A concise description of how the Schnerr-Sauer model works is presented below.

The general form of vapor transport equation can be written as,

$$\frac{\partial}{\partial t}\left(\alpha\rho_v\right)+\nabla\cdot\left(\alpha\rho_v\vec{V}\right)=\frac{\rho_v\rho_l}{\rho}\frac{D\alpha}{Dt}$$

Here, α represents volume fraction of vapor. Also the net mass source term is

$$R=\frac{\rho_v\rho_l}{\rho}\frac{d\alpha}{dt}$$

Schnerr and Sauer use the following expression to connect the vapor volume fraction to the number of bubbles per volume of liquid,

$$\alpha = \frac{n_b \frac{4}{3}\pi \Re_B^{\,3}}{1 + n_b \frac{4}{3}\pi \Re_B^{\,3}}$$

So we have,

$$R = \frac{\rho_v \rho_l}{\rho} \alpha (1-\alpha) \frac{3}{\Re_B} \sqrt{\frac{2}{3} \frac{(P_v - P)}{\rho_l}}$$

$$\Re_B = \left(\frac{\alpha}{1-\alpha} \frac{3}{4\pi} \frac{1}{n} \right)^{\frac{1}{3}}$$

Where, $R =$ mass transfer rate between two phases, $\Re_B =$ bubble radius

This equation can be used for modeling both the evaporation and condensation process. Therefore, the final form can be expressed as follows,

If $P_v \geq P$,

$$R_e = \frac{\rho_v \rho_l}{\rho} \alpha (1-\alpha) \frac{3}{\Re_B} \sqrt{\frac{2}{3} \frac{(P_v - P)}{\rho_l}}$$

Otherwise $P_v \leq P$,

$$R_c = \frac{\rho_v \rho_l}{\rho} \alpha (1-\alpha) \frac{3}{\Re_B} \sqrt{\frac{2}{3} \frac{(P - P_v)}{\rho_l}}$$

III.3 Numerical Algorithm

All the equations listed above are theoretical models governing the whole flow domain. By coupling and calculating these equations can give us the exact solution of parameters distribution, such as pressure, velocity and volume fraction of vapor. However, obviously it is impossible to get the analynical solution to these equations due to the nonlinearity and partial differentiation. Therefore numerical algorithm has to be implemented to make this

calculation plausible. By modeling the cavitation flow in FLUENT, finite volume method is used to discretize the fluid domain into hundreds of thousands of elements. Applying both the initial guess and the boundary conditions, solution of the whole domain is calculated at each iteration and compared to the iteration before until the discrepancy is small enough. Then this calculation is considered converged and the solution should be somewhere near the exact solution. With the help of work station with multiple CUPs, for a pipe incorporated with 2.5m length and 0.1m diameter, resolution as high as 100,000 elements, the whole calculation will take about 1 hour for a turbulent flow condition and 3 hours for a cavitation condition.

III.4 Geometry and Boundary Condition Setup in FLUENT

Inlet pressure and outlet pressure are defined as the boundary conditions. Simply outlet pressure is fixed as atmospheric pressure. Inlet pressure is variable to generate multiple pressure differences. No slip condition is implemented for the pipe wall as well as the orifice plate surfaces. A 2D axisymmetric geometry with $\beta = 0.5$ is shown in Figure 8, in association with boundary condition setup.

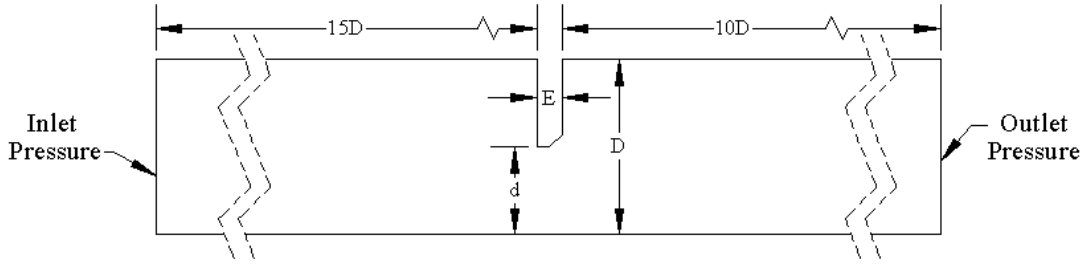

Figure 8 Geometry of fluid domain and boundary condition setup

CHAPTER IV

TURBULENT AND CAVITATION MODEL VALIDATION

As described in the previous chapter, when a FLUENT simulation is carried out, both turbulence model and cavitation model have to be set up in order to simulate the cavitation flow through orifice plate. The governing equations behind the turbulence phenomenon, which consist of continuity equation and Navier-Stokes equation, are absolutely accurate without any doubt. However, the accuracy of these FLUENT models remains skeptical since several major assumptions are made while deriving them. For example, gradient transport hypothesis is applied to derive the k-epsilon turbulence model. Also, for Schnerr-Sauer model, it is derived based on Raylerigh-Plesset's bubble dynamics equation with certain simplification like neglecting the second-order terms and the surface tension force. No strong evidences show the bubble dynamics equation can predict the growth and collapse of water bubbles in the flow for every case, let along the effectiveness of Schnerr-Sauer cavitation model in the orifice flow. Therefore, validations for both turbulence and cavitation models need to be done respectively.

IV.1 Turbulence Model Validation

IV.1.1 Case Description

To validate turbulence model, the experiment data from G. H. Nail's [19] paper is cited. The simulation results are compared with experiment later in this section.

The objective of Nail's study was to increase the knowledge of the flow field present in a typical orifice meter. This was accomplished by using a 3-D LDV (Laser Doppler Velocimeter) to collect detailed 3-D velocity measurements within an orifice meter ($\beta = 0.5, \beta = 0.75$, and $E = 3.2mm, e = 1.6mm$). The working fluid was air at pipe Reynolds numbers of 18,400, 54,700 and 91,100. Reduction of the correlated, instantaneous velocities in three dimensions enabled the calculation of both component mean velocities and previously unavailable complete Reynolds stress tensor. This information was then used to compute a number of other quantities including vorticity,

turbulence kinetic energy, turbulence kinetic energy production rate and correlation coefficients.

To implement similitude method, similar geometry and the same operation conditions need to be defined when conducting numerical study in FLUENT. That means, an orifice plate meter with $\beta = 0.5$ and $\beta = 0.75$ should be modeled and meshed. In addition, the inlet Reynolds number have to be exactly identical with those in experiments. So two cases are chosen for this validation study, which are $\beta = 0.75$, $\mathrm{Re} = 54700$ and $\beta = 0.5$, $\mathrm{Re} = 91100$. Both cases have fixed pressure at outlet of pipe, as much as 1 atm. The geometry and boundary condition setup in FLUENT are shown in Figure 9.

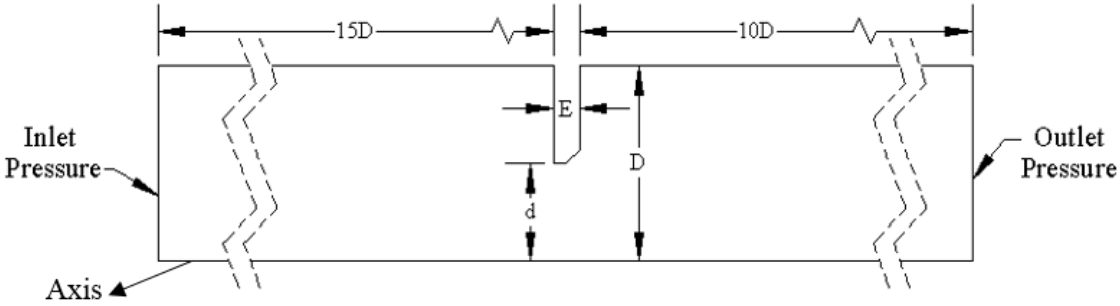

Figure 9 Geometry and boundary condition setup

Regarding the fact that the flow domain within pipe is going to be axisymmetric, it is not necessary to do the whole domain simulation. As a result, only half of a cross-section area is chosen to be the flow domain for purpose of calculation efficiency. To verify the accuracy of the 2D axisymmetric simulation, more details about 3D simulation and 2D axisymmetric simulation comparison will be discussed later.

The mesh is generated by GAMBIT and imported in FLUENT (shown in Figure 10). Only the critical mesh region, the orifice plate region, is shown in the figure due to the excessive length of the pipe. The mesh at orifice throat is densified since there occurs significant pressure and velocity gradient and it might also be the place where cavitation appears. The boundary layers of the flow near the walls also desire finer mesh.

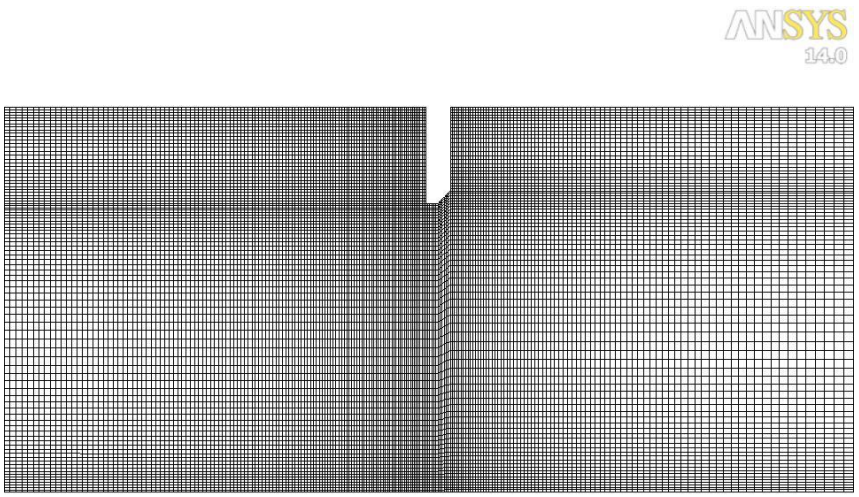

Figure 10 Mesh of flow domain

IV.1.2 Results and Comparison

The simulation of $\beta = 0.75$, $\mathrm{Re} = 54700$ case is first carried out in FLUENT by using k-epsilon model. The profiles of four different parameter are analyzed and compared to the experiment results by Nail. Each of these parameters is non-dimensionalized based on similitude method. When plotting the parameter contours, the whole domain geometry on axial direction is multiplied by a scale factor 0.25 to match the experiment results. The comparison and analysis of each parameter profile is presented in details below.

Figure 11 shows the axial velocity along radial direction at different locations in the pipe. Six locations are selected, one at upstream and five from downstream. All locations are non-dimensionalized and expressed as X/R=-3, X/R=0.25, X/R=0.5, X/R=1, X/R=2, X/R=4, where R is the radius of the pipe. The velocity profiles are compared with those from experiments. Similarly, comparisons are made for the rest of parameters.

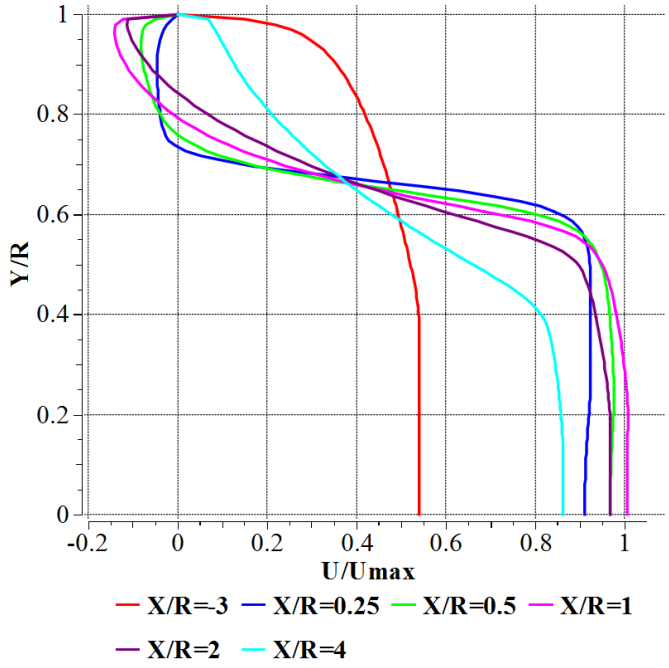

(a) FLUENT simulation result

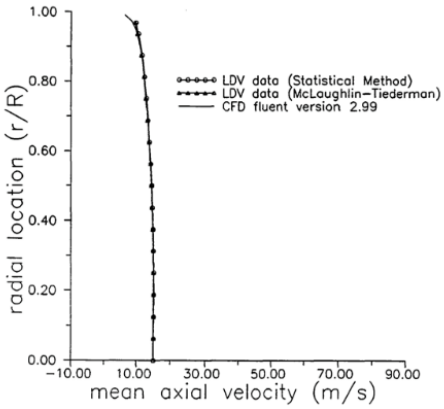

(b) Experiment X/R=-3

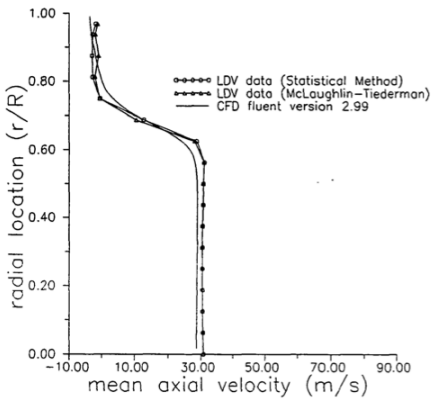

(c) Experiment X/R=0.25

Figure 11 Axial velocity along the radial direction at variable locations in the pipe comparison [19].

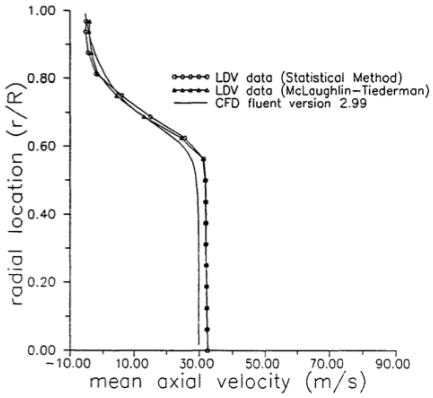

(d) Experiment X/R=0.5

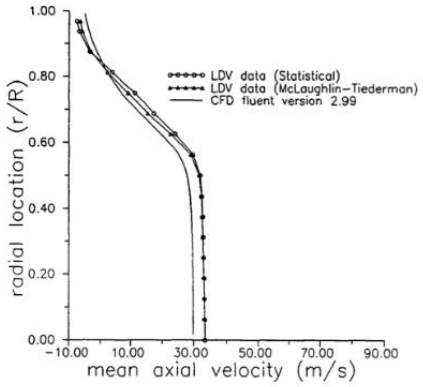

(e) Experiment X/R=1

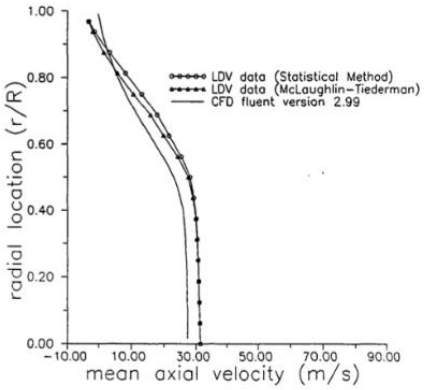

(f) Experiment X/R=2

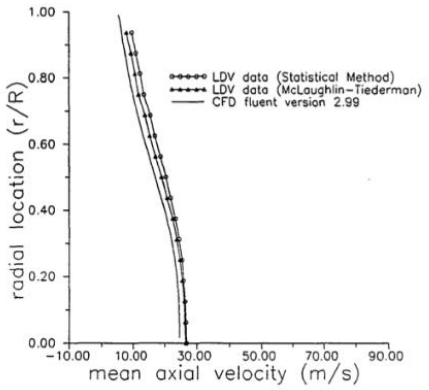

(g) Experiment X/R=4

Figure 11 Contiued

Similarly, Figure 12 shows the normalized axial velocity profile. The velocity is normalized by multiplying $\frac{1}{U_{\max}}$, where $U_{\max}$ is the maximum velocity along axis.

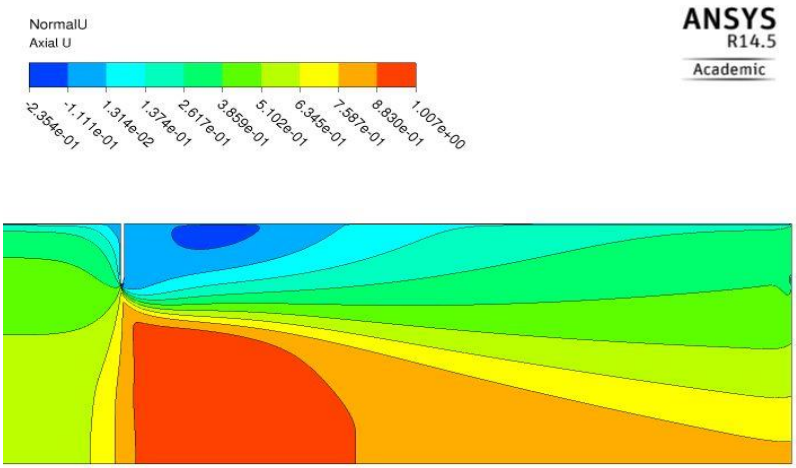

(a) FLUENT simulation

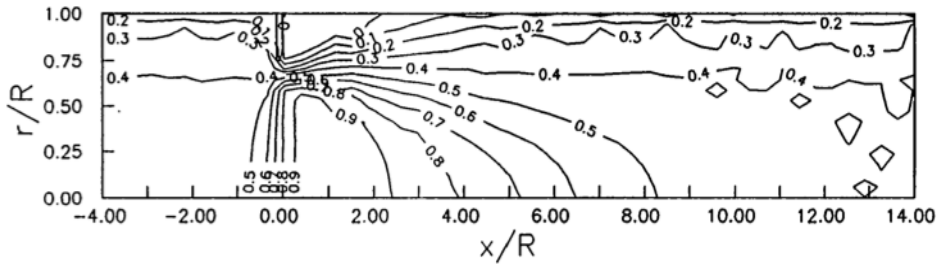

(b) Experiment [19]

Figure 12 Normalized mean axial velocity profile comparison

Figure 13 illustrates the non-dimensional turbulence kinetic energy profile. TKE is non-dimensionalized by multiplying $\frac{100}{U_{\max}^{2}}$.

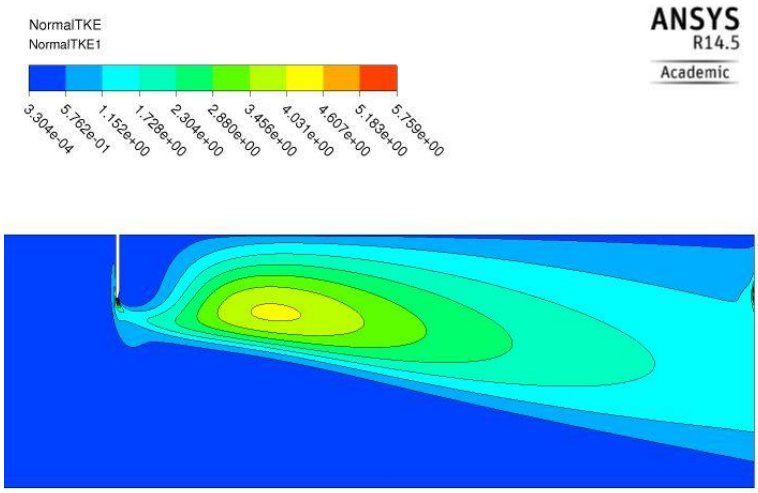

(a) FLUENT simulation

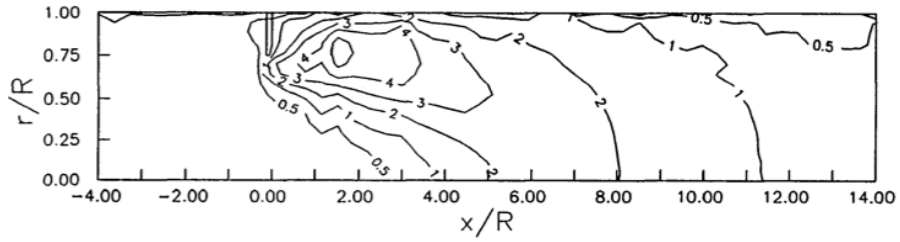

(b) Experiment [19]

Figure 13 Non-dimensional turbulence kinetic energy profile comparison

The non-dimensional vorticity profile is shown in Figure 14. Vorticity is non-dimensionalized by multiplying $\frac{R}{U_{\max}}$, where R is radius of pipe

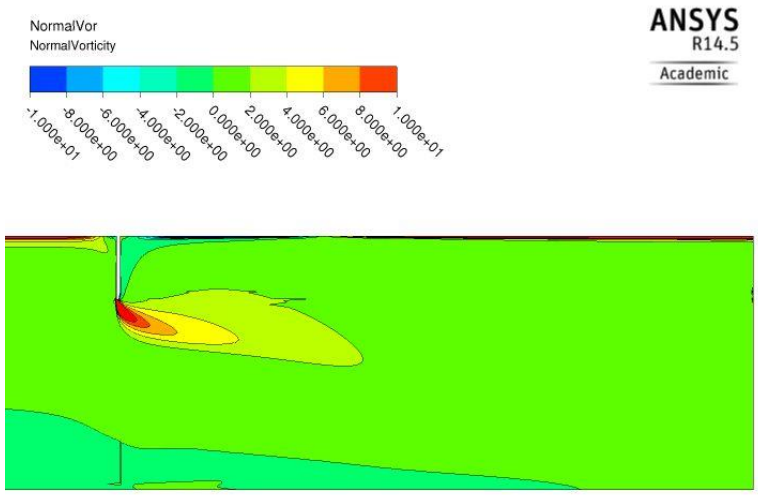

(a) FLUENT simulation

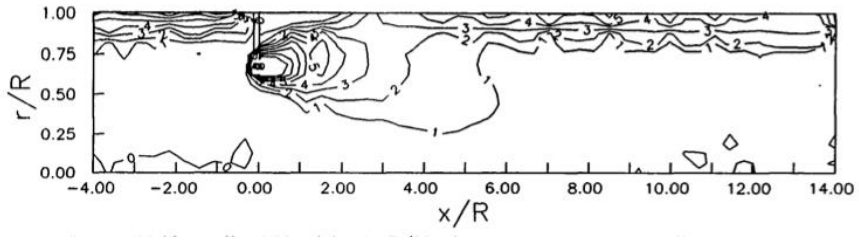

(b) Experiment [19]

Figure 14 Non-dimensional vorticity profile comparison

From the comparisons, FLUENT simulation can present nearly the same information as experiments only with more details and higher resolution. As for radial velocity profile in Figure 11, simulation can perfectly predict the velocity profile along radial direction at different locations downstream. Though the experiment results are in absolute value, the shape of the curves still resemble each other. This leads to a further corollary that the whole velocity distribution in the flow domain predicted by simulation is going to be identical with the experiment results, which is thoroughly proved in Figure 12. Other parameter distributions of both simulation and experiments, such as turbulence kinetic energy and vorticity, also show extreme similarity. So far, conclusion can be made that by using k-epsilon model, relatively accurate results can be obtained regarding different

turbulent features for a 2D axisymmetric geometry. However, question may raise that how it is different from 3D simulation? Can we directly use 3D simulation which seems to be more straightforward and realistic? The answer to these questions will be present in the following paragraphs.

Analysis and comparison of case $\beta = 0.5$, $\mathrm{Re} = 91100$ between experiment and simulation are performed. In this case, velocity distribution along axis and wall pressure is added in comparison. Besides, comparison between 2D axisymmetric and 3D results is also carefully considered at this section. Intuitively speaking, usually a single steady state fully converged 3D simulation case in FLUENT can cost up to 10 hours' time and 1 GB memory space of computer, depending on the geometry complexity and mesh density. A transient study can take even longer. If the geometry can be simplified or mesh can be coarser without sacrifice the accuracy of results, it is going to be a giant improvement of the simulation and becomes more time and cost efficient. That is what motivates me to do the 2D axisymmetric and 3D simulation comparison.

The geometry and mesh of 3D flow domain is illustrated below (Figure 15).

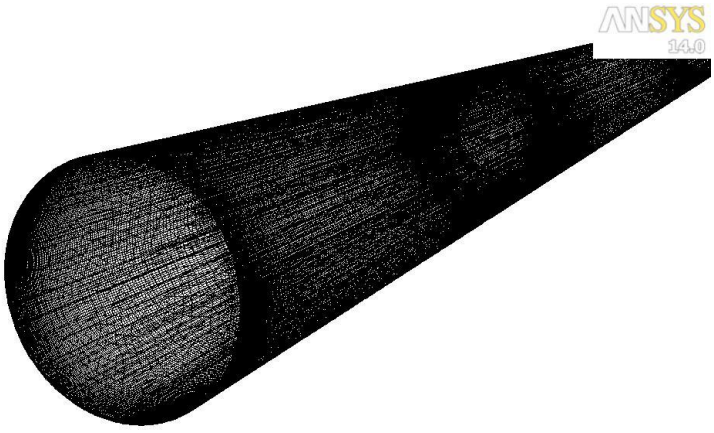

Figure 15 Geometry and mesh of 3D model

Several parameters distribution in terms of 2D axisymmetric, 3D simulation and experiments for case, $\beta = 0.5$, $\mathrm{Re} = 91100$, are analyzed and compared as below (Figure 16,Figure 17,Figure 18,Figure 19).

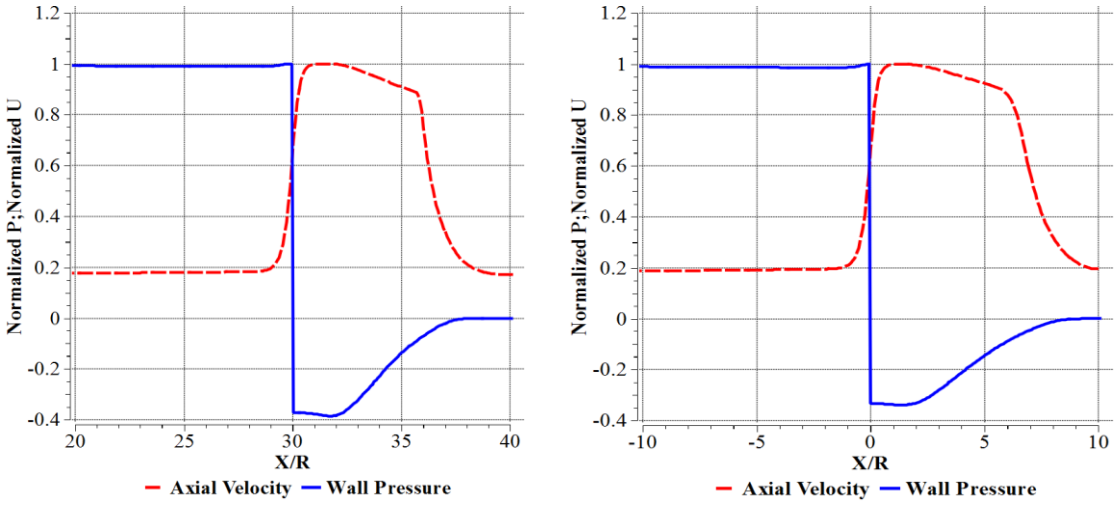

(a) 2D axisymmetric (b) 3D

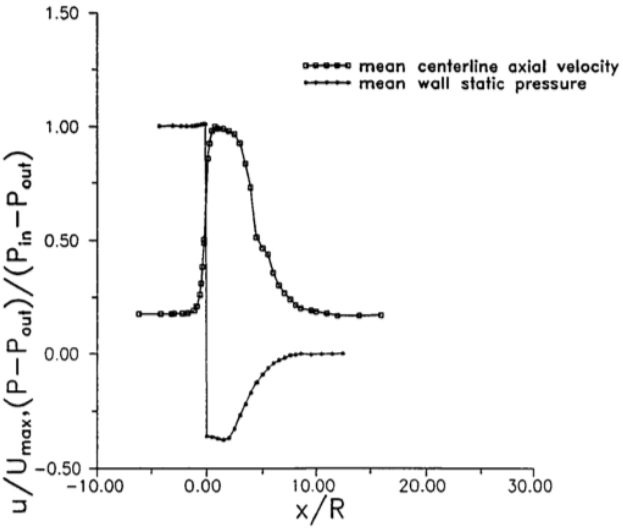

(c) Experiment [19]

Figure 16 Normalized pressure and velocity comparison

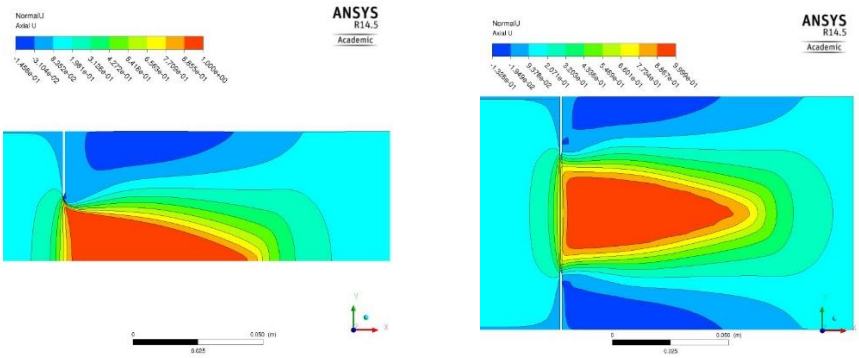

(a) 2D axisymmetric (b) 3D

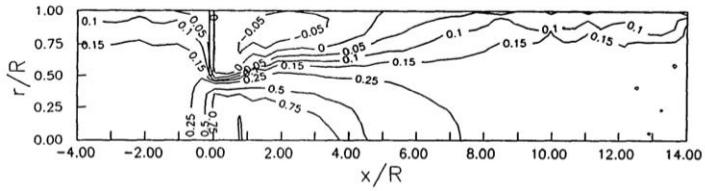

(c) Experiment [19]

Figure 17 Normalized mean axial velocity profile comparison

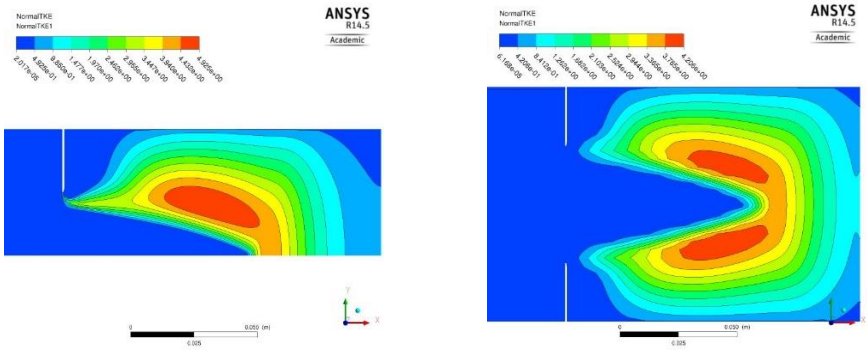

(a) 2D axisymmetric (b) 3D

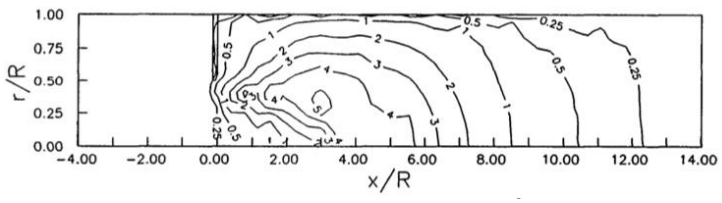

(c) Experiment [19]

Figure 18 Non-dimensional TKE comparison

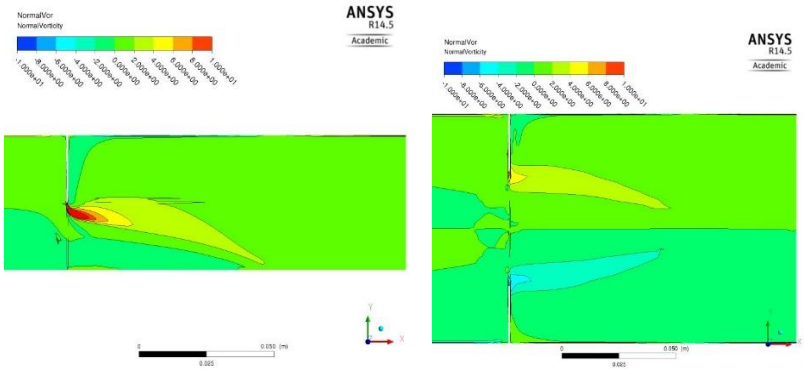

(a) 2D axisymmetric (b) 3D

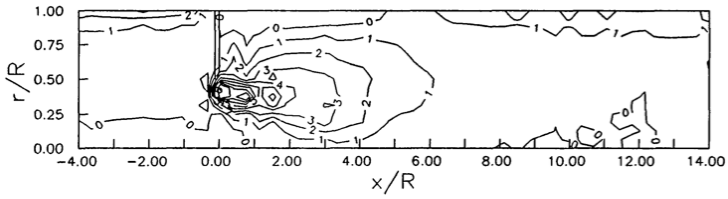

(c) Experiment [19]

Figure 19 Non-dimensional vorticity comparison

Comparing to experiment data, FLUENT can offer us quite accurate location along the axis of pipe where the maximum and minimum velocity and pressure occur. As a consequence, the exact location of vena-contracta is able to be revealed by FLUENT simulation. From the pressure profile along the axis, other information can be gathered like the reattachment location of the flow at downstream, which is roughly identical in both experiment and simulation results (Figure 16). Also, FLUENT can give us results of TKE and vorticity distribution within acceptable tolerance of error (see Figure 18, Figure 19). Since pressure profile, velocity profile, TKE and vorticity distribution are all we need out of turbulence model when doing cavitation study later on, if the experiment data from Nail is trustworthy, conclusion can be made that k-epsilon can be used for cavitation study.

Moreover, Table 2 shows comparison of basic simulation statistics for 2D axisymmetric and 3D simulation. From this table, P_{max} value of 2D axisymmetric only deviate from 3D result by 0.6%, while U_{max} differentiates by 4.5%. Also, we can easily notice the normalized results between 2D axisymmetric and 3D are so similar that discrepancies can be neglected (Figure 16, Figure 17, Figure 18, and Figure 19). However, 2D axisymmetric is much superior than 3D in terms of cell number and time cost. 3D simulation has nearly 20 times the cell number 2D axisymmetric has. But 2D axisymmetric only takes 1/40 time 3D simulation does. Therefore, 2D axisymmetric method is applied in future cavitation study.

Table 2 Comparison of simulation statistics for 2D axisymmetric and 3D simuation

case	Mesh cell number	Time cost (hr.)	P_{max} (Pa)	U_{max} (m/s)
2D axisymmetric	67000	0.5	113000	5.82
3D	1500000	20	112300	5.57

IV.2 Cavitation Model Validation

IV.2.1 Case Description

Apart from turbulence model validation mentioned in previous section, cavitation model validation is also very important since it will be applied for all future cavitation study. The experiment data from W. H. Nurick [2] is cited to compare with FLUENT simulation results. Schnerr-Sauer cavitation model is selected. Same geometry and boundary condition as experiment are defined in simulation. Similarly, a 3D simulation case is also evaluated in purpose of verifying the accuracy of 2D axisymmetric simulation.

Nurick's paper provides insight into the mechanisms predicting and controlling cavitation in sharp-edged orifice. Within his experiment, a variety of single orifices, including those fabricated from Lucite, stainless steel and aluminum, were used to determine cavitation characteristics. The entrance sharpness tolerances were maintained to 0.003 in. Static pressure taps were incorporated in the wall of the orifices at ¼ and ½ diameter downstream of the inlet. The tap closest to the inlet is at the approximate location of the vena contract and tap at ½ diameter downstream is within the recompression zone. Among all these orifice, one with $D/d = 2.88, L'/D = 5$ is selected for simulation study. The geometry of this orifice and mesh are shown below (Figure 20).

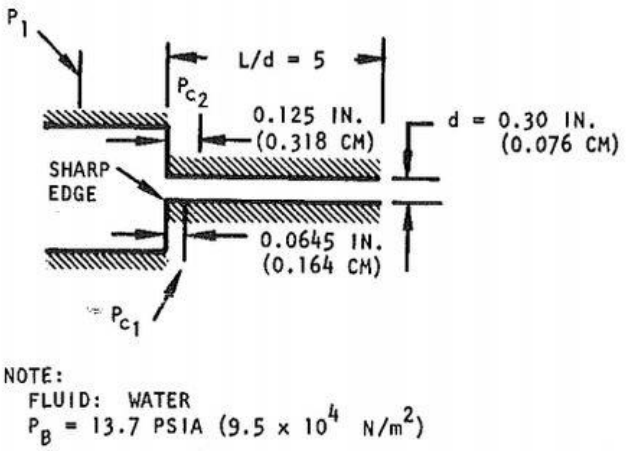

(a) Geometry and dimensions[2]

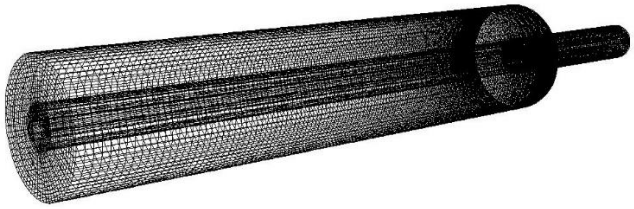

(b) 3D geometry and mesh

Figure 20 Geometry and mesh of the orifice

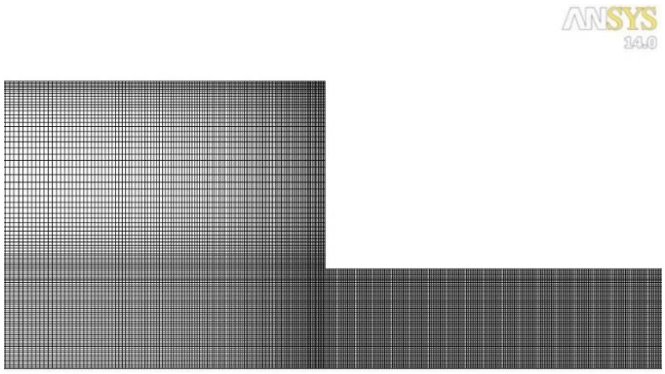

(c) 2D axisymmetric geometry and mesh

Figure 20 Continued

IV.2.2 Results and Comparison

Both inlet pressure P_1 and outlet pressure P_b boundary condition are defined. Outlet pressure is fixed at 13.7 psi while inlet pressure is variable from 15 psi to 40 psi. Water is chosen to be the fluid medium. Results for each inlet pressure are recorded and put together to make two different plots. First plot is change of downstream wall pressure in terms of inlet pressure (see Figure 21). Second is plot of discharge coefficient vs cavitation index (see Figure 22).

Discharge coefficient is defined as

$$Cd = \frac{\dot{m}}{A\sqrt{2(P_1 - P_b)\rho}}$$

Where $\dot{m}$ is the actual mass flow rate within the orifice; A is the cross section area of the orifice.

At the same time, cavitation index is defined as

$$Ca = \frac{P_1 - P_v}{P_1 - P_b}$$

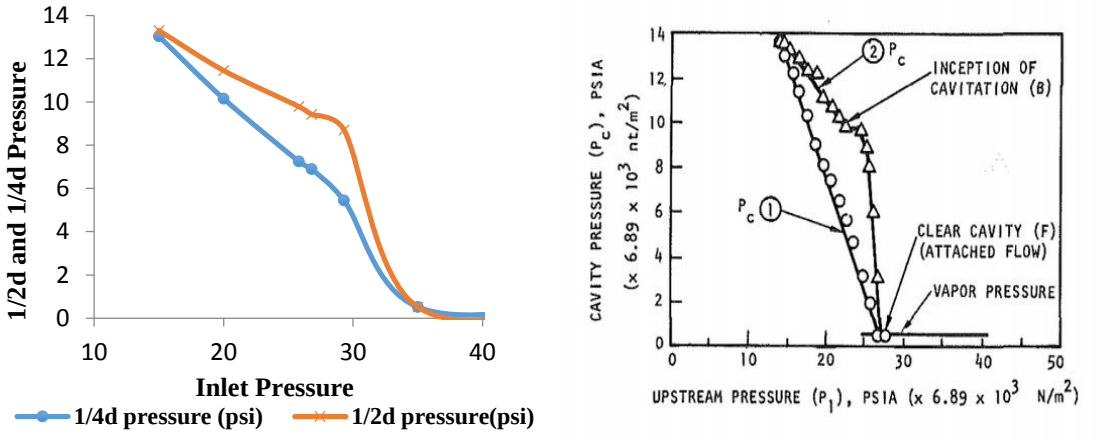

(a) Simulation (b) Experiment

Figure 21 Experiment [2] and simulation results of downstream wall pressure vs inlet pressure

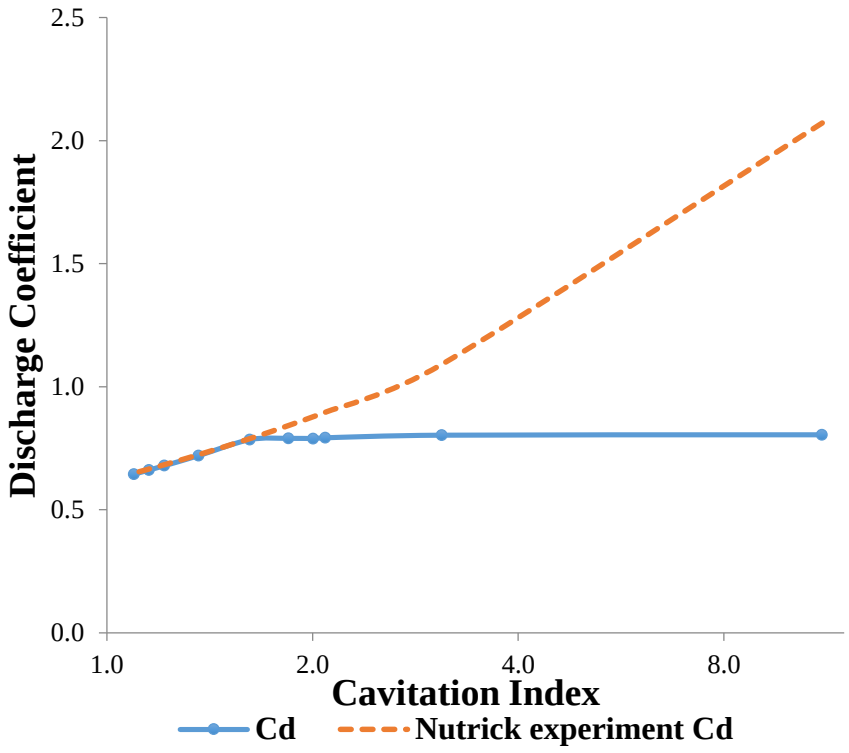

Figure 22 Discharge coefficient vs cavitation number

The dash line above (Figure 22) represents the experiment result by Nurick. Only the left end of the dash line, at cavitation index from 1.0 to 2.0, really matters and shows us how discharge coefficient changes along with cavitation number. This portion of dash line is governed by the equations below which are summarized and correlated based on huge amount of experiment data.

$$C_c = 0.62 + 0.38\,(A_1/A_0)^3$$

$$C_D = C_c \left(\frac{P_1 - P_v}{P_1 - P_B} \right)^{1/2}$$

From the plot of downstream wall pressure as a function of the inlet pressure (Figure 21), a linear reduction of pressure is observed at ¼ diameter pressure tap, showing vena-contracta is at or near this location. The tap at ½ diameter also initially drops linearly but has higher absolute pressure showing that it is within the liquid recompression zone. As the upstream pressure is further increased, the pressure at ½ diameter tap reaches a plateau region, which is believed to correspond to the pressure where cavitation occurs. The simulation result indicates both vena-contracta and recompression zone are located at exact same places as they are in experiment. It also shows the plateau happens at about 30psi of inlet pressure. Even though 30psi is higher than 25psi from experiment, it is still reasonable since water used in experiment has certain amount of gas dissolved in it, which makes it easier to cavitate with less restricted pressure requirement.

The simulation result of discharge coefficient as a function of cavitation index matches the result from experiment perfectly (Figure 22). At large cavitation index region, discharge coefficient is almost invariant. As the cavitation index decreases to 1.5, discharge coefficient begins to drop. The gradient of that dropping slope coincides with the dash line governed by the empirical correlations.

Therefore, conclusion can be made that the cavitation model of FLUENT can provide us with relatively accurate results.

For the 3D simulation case, a specific boundary condition is set up as inlet pressure equals to 50 psi, outlet pressure still fixed at13.7 psi. The mass flow rate and maximum velocity of both 2D axisymmetric and 3D simulation are compared and presented in Table 3.

Table 3 Comparison of simulation statistics of 2D axisymmetric and 3D

Case	Mesh cell number	Time cost (hr.)	Mass flow rate (kg/s)	Maximum velocity (m/s)
2D axisymmetric	35578	0.3	0.735	26.15
3D	519522	5	0.723	26.1

Profiles of pressure and velocity along the centerline are plotted for both 2D axisymmetric and 3D simulation (see Figure 23). Both pressure and velocity are normalized by being divided by the maximum value of each on centerline. Besides, the vapor volume fraction contour is presented and compared in Figure 24.

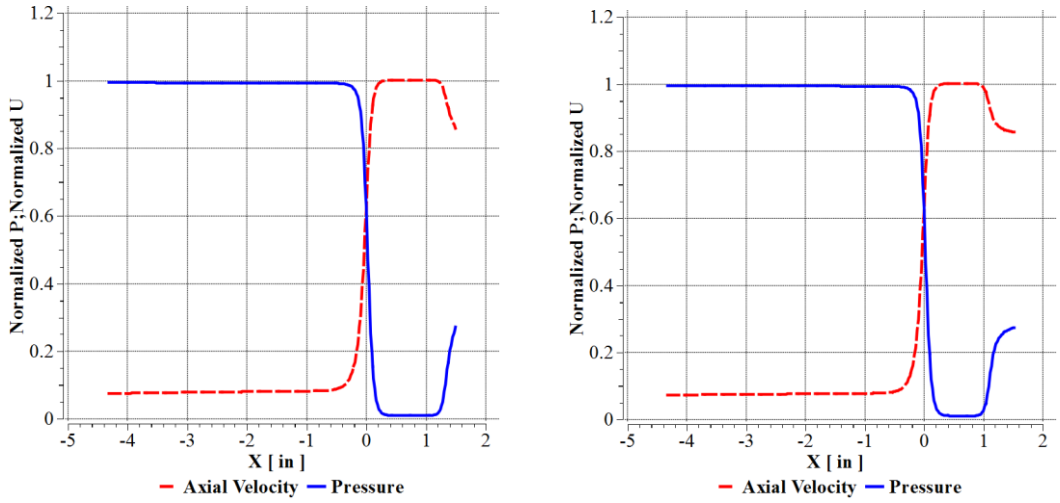

(a) 2D axisymmetric (b) 3D

Figure 23 Normalized pressure and axial velocity distribution along centerline

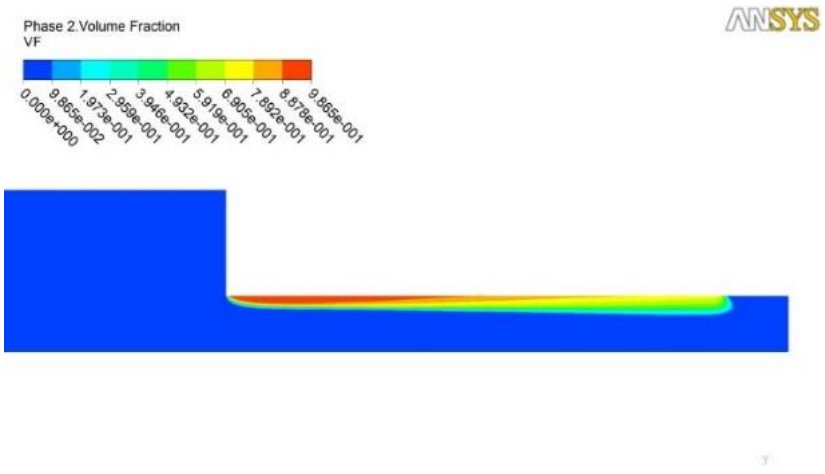

(a) 2D axisymmetric simulation

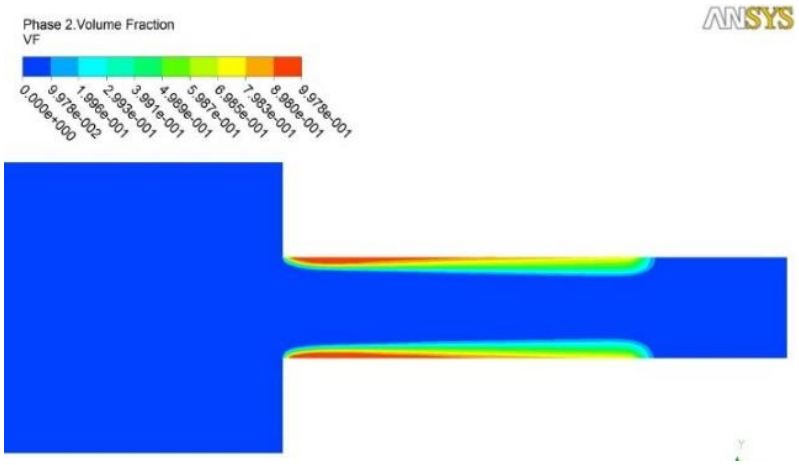

(b) 3D

Figure 24 Vapor volume fraction contour comparison

From the simulation efficiency study, 2D axisymmetric method can simulate the same flow case within much less time (Table 3), but still offer nearly the same result as 3D simulation. To further back up this conclusion, Figure 23 gives us insight of how the velocity and pressure profile in 2D axisymmetric simulation match that from 3D simulation. Also, to get a more general view, the vapor volume fraction contour of 2D axisymmetric is extremely similar with that from 3D. Given the superiority of 2D axisymmetric method, it further reinforces the application of 2D axisymmetric in cavitation study.

CHAPTER V

NON-DIMENSIONALIZATION STUDY

To understand a flow system like orifice flow, all parameters within this system who have certain effects on the flow features need to be correlated. Therefore, in this case, parameters can be categorized into three group: geometry parameters, fluid properties parameters and operating conditions. Geometry has parameters like pipe diameter D , orifice throat diameter d . Fluid properties contain parameters like density ρ and viscosity μ . Meanwhile, operating conditions like inlet pressure P_1, outlet pressure P_2 need to be set up to run the simulation.

Non-dimensionalization study can help to dramatically simplify the flow system by reducing variables associated with the system. In addition, non-dimentsionalization study can eliminate the scale effects, which makes the similitude possible. Anyone, at any time, using any fluid medium, should be able to obtain very similar simulation results if all non-dimensional parameters remain the unchanged. This gives us more general perception of what really controls the flow features.

Given all the advantages of non-dimensionalization, each parameter within this system need to be non-dimensionlized by applying the Buckingham Pi Theorem. This process is presented below:

(1). The inlet mean velocity u is a function of several parameters, including D , d , P_2 , ΔP_v , ρ , μ . So the relation could be written as,

$$u = f(D, d, P_2, \Delta P_v, \rho, \mu)$$

Where, $\Delta P_v = P_1 - P_v$, P_v represents vapor pressure.

Also, the pressure difference between the orifice throat and inlet $\Delta P_o = P_1 - P_o$ is a function of D, d, P_1, P_2, ρ, μ. The relation can be expressed as,

$$\Delta P_o = g(D, d, P_1, P_2, \rho, \mu)$$

(2). Among all seven parameters, three are selected with fundamental physical dimensions in them. These three are D, u, ρ for the first relation and D, P_2, ρ for the second relation. That leaves the other four to possess the ability to be non-dimensional parameters.

(3). After applying the Buckingham Pi Theorem, four non-dimensional parameters are generated and shown below.

$$\frac{P_2}{\rho u^2} = f\left(\frac{d}{D}, \frac{\Delta P_v}{\frac{1}{2}\rho u^2}, \frac{\mu}{\rho u D}\right)$$

$$\frac{\Delta P_o}{P_2} = g\left(\frac{d}{D}, \frac{P_1}{P_2}, \frac{\mu}{\rho^{\frac{1}{2}} D P_2^{\frac{1}{2}}}\right)$$

Where, diameter ratio $\beta = \frac{d}{D}$, cavitation number $\sum = \frac{\Delta P_v}{\frac{1}{2}\rho u^2}$, inverse of Reynolds number is $\frac{1}{\mathrm{Re}} = \frac{\mu}{\rho u D}$, pressure ratio $\frac{P_1}{P_2}$.

Moreover, if we multiply these two relations with each other, yields,

$$\frac{1}{Cd} = \sqrt{\frac{\Delta P_o}{\rho u^2}} = \frac{A_o\sqrt{2\Delta P_o \rho}}{\dot{m}} = \sqrt{f\left(\frac{d}{D}, \frac{\Delta P_v}{\frac{1}{2}\rho u^2}, \frac{\mu}{\rho u D}\right) \times g\left(\frac{d}{D}, \frac{P_1}{P_2}, \frac{\mu}{\rho^{\frac{1}{2}} D P_2^{\frac{1}{2}}}\right)}$$

Within this new relation, Cd means discharge coefficient of the orifice plate. $\dot{m}$ is the mass flow rate of the pipe, and A_0 is the cross section area of the orifice throat.

From this final form of correlation, we know that discharge coefficient of the orifice plate is a function of several non-dimensional parameters, including diameter ratio, Reynold's number and cavitation number etc.

CHAPTER VI

RESULTS AND DISCUSSIONS

VI.1 Steady State Study of Cavitation Effect on Discharge Coefficient

An orifice plate is a device used for measuring flow rate, reducing pressure or restricting flow. Either a volumetric or mass flow rate may be determined, depending on the calculation associated with the orifice plate. It uses the same principle as a Venturi nozzle, namely Bernoulli's principle which states that there is a relationship between the pressure of the fluid and the velocity of the fluid. When the velocity increases, the pressure decreases and vice versa.

Orifice plates are most commonly used to measure flow rates in pipes. Under the circumstances when the fluid is single-phase rather than being a mixture of gases and liquids, or of liquids and solids, when the flow is continuous rather than pulsating, when the flow profile is even and well-developed, when the fluid and flow rate meet certain other conditions, and when the orifice plate is constructed and installed according to appropriate standards, the flow rate can easily be determined using published formulae based on substantial research.

Once the orifice plate is designed and installed, the flow rate can often be indicated with an acceptably low uncertainty simply by taking the square root of the differential pressure across the orifice's pressure tappings and applying an appropriate constant. Even compressible flows of gases that vary in pressure and temperature may be measured with acceptable uncertainty by merely taking the square roots of the absolute pressure and/or temperature, depending on the purpose of the measurement and the costs of ancillary instrumentation.

There are three standard positions for pressure tappings, commonly named as follows:

(1). Corner taps placed immediately upstream and downstream of the plate; convenient when the plate is provided with an orifice carrier incorporating tappings

(2). D and D/2 taps or radius taps placed one pipe diameter upstream and half a pipe diameter downstream of the plate; these can be installed by welding bosses to the pipe

(3). Flange taps placed 25.4mm (1 inch) upstream and downstream of the plate, normally within specialized pipe flanges.

Usually when Reynolds number is larger than 10000, the discharge coefficient of the orifice plate is nearly constant, no longer dependent on Reynolds number within the pipe. At this time, discharge coefficient is only function of the diameter ratio and the pressure tapping type. The empirical function is based on a huge amount of substantial research and can be expressed as,

$$Cd = 0.5961 + 0.0261\beta^2 - 0.216\beta^8 + (0.043 + 0.080e^{-10L_1} - 0.123e^{-7L_1})\frac{\beta^4}{1-\beta^4} - 0.031(M_2' - 0.8M_2'^{1.1})\beta^{1.3}$$

Where, $M_2' = \dfrac{2L_2'}{1-\beta}$

Only three following pairs of values for L_1 and L_2' are valid:

(1). Corner tappings: $L_1 = L_2' = 0$

(2). Flange tappings: $L_1 = L_2' = \dfrac{0.0254}{D}$

(3). D and D/2 tappings: $L_1 = 1, L_2' = 0.47$

Once the orifice diameter ratio and pressure tapping method are determined, as long as Reynolds number is big enough, discharge coefficient can be easily calculated by using the empirical function above. As a sequence, the mass flow rate can be determined by the following equation,

$$\dot{m} = Cd \cdot A_o \cdot \sqrt{2(P_D - P_{D/2})\rho}$$

In which, A_0 represents orifice throat area; P_D means the pressure one diameter upstream and $P_{D/2}$ is the pressure at D/2 downstream.

Above describes how a standard orifice plate fulfills its duty as a mass flow rate meter. However, the recommended working condition for these orifice plates is single-phase flow rather than being a mixture of gases and liquids, or of liquids and solids. So problem rises as when Reynolds number increases to certain point, cavitation occurs inevitably. This makes the flow a two-phase flow. It is uncertain what effects cavitation will bring to the discharge coefficient of the orifice plate, neither can we say the meter can still work properly. Also experiments show that as cavitation keeps growing, the flow within the pipe will reach chocked stage, even super cavitation stage. These intense and highly uncertain flow phenomenon may influence the flow pattern more or less. Therefore, in this section, numerical investigation regarding cavitation effect on discharge coefficient will be performed. Moreover, the incipient cavitation number will be determined for each diameter ratio

VI.1.1 Case Description

To get a general idea of cavitation effects, orifice plates with diameter ratio from 0.2 to 0.75 are selected and modeled in FLUENT. The pipe in which orifice plate is located, need to be long enough in order to have fully developed turbulence flow upstream the orifice. So the distance from inlet to front surface of orifice is 15 times diameter, while downstream length is 10 times diameter to help capture all flow features (see Figure 8). For each diameter ratio, several cases are run to simulate flow field at different pressure difference. The outlet pressure is fixed at 1atm in all cases while the inlet pressure gradually increases. Precaution need to be taken that the initial inlet pressure of pipe has to be high enough to guarantee turbulence flow and also low enough to avoid cavitation. Only so, incipient cavitation number can be detected.

Since the turbulence model and the cavitation model have been validated in previous section, k-epsilon model and Schnerr-Sauer are able to be implemented in FLUENT. 2D

axisymmetric simulation is used in regard of time efficiency. D and D/2 pressure tapping method is applied to calculate the value of discharge coefficient.

VI.1.2 Results and Discussion

The results of the cavitation number and discharge coefficient are shown in several tables below, where cavitation number is defined as

$$\sum = \frac{P_o - P_v}{\frac{1}{2}\rho u^2}$$

Where, u and P_o are the mean flow velocity and pressure at orifice. Both the cavitation number and discharge coefficient are rounded to three decimal places.

Table 4 $\beta = 0.2$

β	P_1	P_2	P_D	$P_{D/2}$	$\dot{m}$	$\sum$	Cd	Cavitation?
0.2	105000	101000	105000	3540	2.75	2.536	0.614	YES
0.2	110000	101000	110000	3540	2.816	2.420	0.614	YES
0.2	150000	101000	150000	3540	3.3	1.768	0.614	YES
0.2	200000	101000	200000	3540	3.82	1.310	0.613	YES
0.2	300000	101000	300000	3540	4.7	0.866	0.614	YES
0.2	350000	101000	350000	3540	5.08	0.743	0.614	YES
0.2	400000	101000	400000	3540	5.43	0.649	0.614	YES

Table 5 $\beta = 0.3$

β	P_1	P_2	P_D	$P_{D/2}$	$\dot{m}$	$\sum$	Cd	Cavitation?
0.3	340000	101000	339000	102000	9.6	1.054	0.624	NO
0.3	350000	101000	349000	87100	10.11	0.949	0.625	NO
0.3	360000	101000	359000	73200	10.56	0.871	0.625	YES
0.3	500000	101000	498000	55500	13.05	0.570	0.620	YES
0.3	600000	101000	598000	44000	14.54	0.459	0.618	YES
0.3	650000	101000	648000	45150	15.16	0.423	0.618	YES
0.3	800000	101000	797000	23200	17.17	0.332	0.617	YES
0.3	900000	101000	896000	8330	18.33	0.289	0.615	YES

Table 6 $\beta = 0.4$

β	P_1	P_2	P_D	$P_{D/2}$	$\dot{m}$	$\sum$	Cd	Cavitation?
0.4	300000	101000	297000	67200	16.81	1.086	0.624	NO
0.4	350000	101000	346800	59000	18.786	0.869	0.623	YES
0.4	400000	101000	396000	41800	20.77	0.711	0.621	YES
0.4	450000	101000	445000	29500	22.454	0.608	0.620	YES
0.4	500000	101000	494000	19600	23.974	0.534	0.619	YES
0.4	600000	101000	593000	3540	26.805	0.427	0.621	YES
0.4	650000	101000	642000	3540	27.95	0.393	0.622	YES
0.4	800000	101000	790000	3540	31.04	0.318	0.623	YES

Table 7 $\beta = 0.5$

β	P_1	P_2	P_D	$P_{D/2}$	$\dot{m}$	$\sum$	Cd	Cavitation?
0.5	250000	101000	245000	72400	23.17	1.390	0.635	NO
0.5	275000	101000	268000	58500	25.57	1.146	0.636	YES
0.5	300000	101000	292000	31800	28.347	0.932	0.633	YES
0.5	350000	101000	340000	14500	31.58	0.750	0.630	YES
0.5	400000	101000	388000	3540	34.37	0.662	0.631	YES
0.5	450000	101000	437000	3540	36.6	0.634	0.633	YES
0.5	500000	101000	485000	3540	38.6	0.559	0.634	YES

Table 8 $\beta = 0.6$

β	P_1	P_2	P_D	$P_{D/2}$	$\dot{m}$	$\sum$	Cd	Cavitation?
0.6	215000	101000	204000	42000	33.5	1.385	0.658	NO
0.6	225000	101000	213000	35000	35.1	1.259	0.658	YES
0.6	250000	101000	235000	22000	38.4	1.052	0.658	YES
0.6	300000	101000	281000	3540	44.04	0.800	0.661	YES
0.6	350000	101000	328000	3540	47.73	0.681	0.663	YES
0.6	400000	101000	375000	3540	51.05	0.596	0.662	YES
0.6	2750000	101000	2580000	3540	134.1	0.086	0.661	YES

Table 9 $\beta = 0.75$

β	P_1	P_2	P_D	$P_{D/2}$	$\dot{m}$	$\sum$	Cd	Cavitation?
0.75	180000	101000	155000	41200	50.5	1.487	0.758	NO
0.75	185000	101000	158000	37200	52.1	1.396	0.759	YES
0.75	200000	101000	169000	25600	56.47	1.190	0.755	YES
0.75	225000	101000	186000	4870	63.2	0.949	0.752	YES
0.75	230000	101000	190000	3540	64.26	0.917	0.753	YES
0.75	235000	101000	194000	3540	65.06	0.895	0.755	YES
0.75	240000	101000	198000	3540	65.87	0.874	0.756	YES
0.75	250000	101000	206000	3540	67.4	0.834	0.758	YES
0.75	300000	101000	247000	3540	73.9	0.695	0.758	YES
0.75	350000	101000	288000	3540	79.8	0.595	0.757	YES

Plot of discharge coefficient in terms of cavitation number for each diameter ratio is shown in Figure 25,

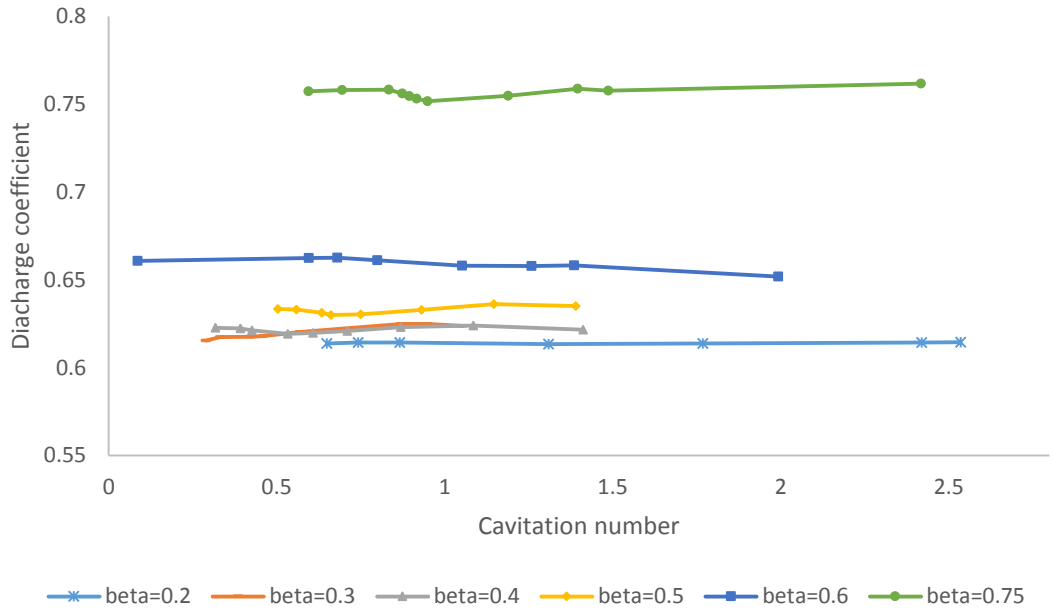

Figure 25 Simulation result of the discharge coefficient in terms of cavitation number and diameter ratio

The first thing we notice from the plot is the discharge coefficient of the orifice plate is nearly independent of cavitation number once the diameter ratio is fixed. This result matches Numachi's experiment [11], as it presents in Figure 26 below.

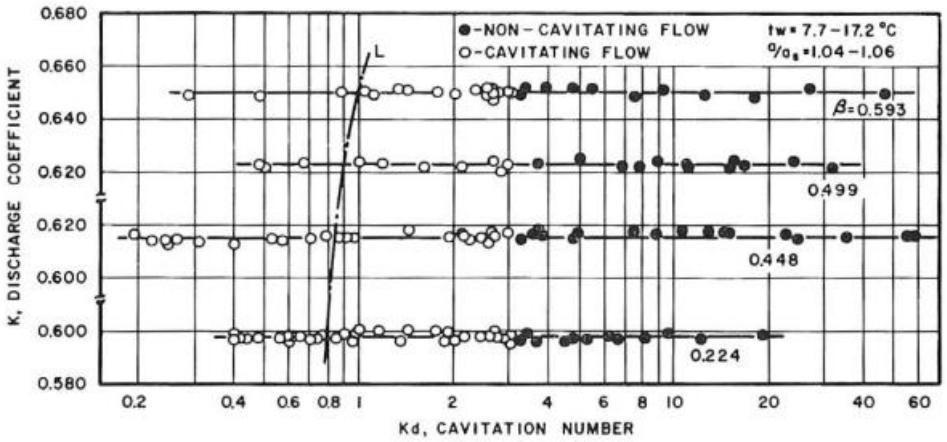

Figure 26 Experiment result of the discharge coefficient in terms of cavitation number and diameter ratio [11].

Apart from the research of cavitation number effects on discharge coefficient, Numachi also conducted experiments to investigate the effects of the inlet Reynolds number and diameter ratio on discharge coefficient. As a result, similar conclusion is obtained, which indicates discharge coefficient of the orifice plate is a constant value for a specific diameter ratio (see Figure 27).

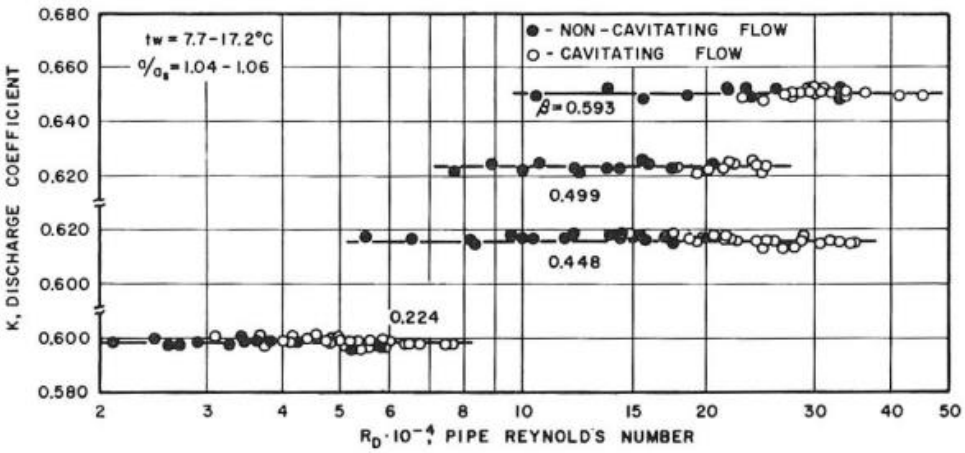

Figure 27 Experiment result of the discharge coefficient in terms of inlet Reynold's number and diameter ratio[11].

Therefore, in associated with the non-dimensionalization study, a simply correlation between discharge coefficient and diameter ratio can be derived as below,

$$\frac{1}{Cd} = \sqrt{\frac{\Delta P_o}{\rho u^2}} = \frac{A_o\sqrt{2\Delta P_o \rho}}{\dot{m}} = \sqrt{f(\frac{d}{D}, \frac{\Delta P_v}{\frac{1}{2}\rho u^2}, \frac{\mu}{\rho u D}) \times g(\frac{d}{D}, \frac{P_1}{P_2}, \frac{\mu}{\rho^{\frac{1}{2}} D P_2^{\frac{1}{2}}})}$$

Given the fact that discharge coefficient Cd is independent of both

$$\sum = \frac{\Delta P_v}{\frac{1}{2}\rho u^2} \text{ and } \frac{1}{\mathrm{Re}} = \frac{\mu}{\rho u D},$$

also that Cd is independent of the inlet pressure P_1 since the altering cavitation number comes from P_1 changes. Besides, the outlet pressure P_2 and the pipe diameter D are constant. So, for a specific material like water incorporated with D and D/2 pressure tapping method, discharge coefficient is a function of and only a function of diameter ratio β. Table 10 below shows how discharge coefficient is related to diameter ratio.

Table 10 Discharge coefficient value for each diameter ratio

β	Cd
0.2	0.614
0.3	0.62
0.4	0.622
0.5	0.633
0.6	0.66
0.75	0.756

Using the polynomial regression, a third degree correlation can be estimated with residual sum of squares 5.17×10^{-7},shown below,

$$Cd = 0.5542 + 0.5626\beta - 1.652\beta^2 + 1.68\beta^3$$

This regression polynomial can be used to estimate discharge coefficient at different diameter ratio.

Other information can be gathered from the simulation, which is no longer match the results of Numachi (Figure 26). The inception cavitation number for each diameter ratio is not fixed as shown in Numachi's experiments, instead, their correlation can be expressed as below (Table 11,Figure 28).

Table 11 Cavitation inception number for various diameter ratio

β	Cavitation inception number
0.3	0.870
0.4	0.870
0.5	1.146
0.6	1.259
0.75	1.340

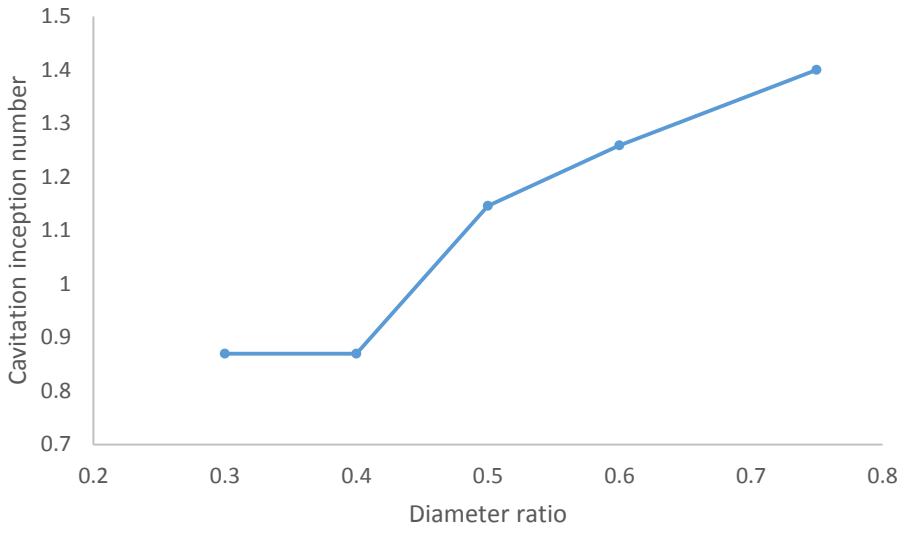

Figure 28 Plot of cavitation inception number vs diameter ratio

Besides Numachi, many other researchers such as Tullis, Govindarajan and Yan have conducted similar experiments to investigate the relationship between cavitation inception number and diameter ratio. Similar trend is shown in their experiment results where cavitation inception number increases with the diameter ratio (Figure 29). However, the cavitation inception numbers reported by Tullis and Govindarajan are generally higher than those observed in Yan's study for particular diameter ratio. This is due to the fact that in Yan's study the pipe diameter is 37.5 mm, whereas the pipe diameters in Tullis and Govindarajan's work are 78 mm and 154 mm. So conclusion can be made that the cavitation inception number has significant size scale effect and it is not simply a function of diameter ratio alone.

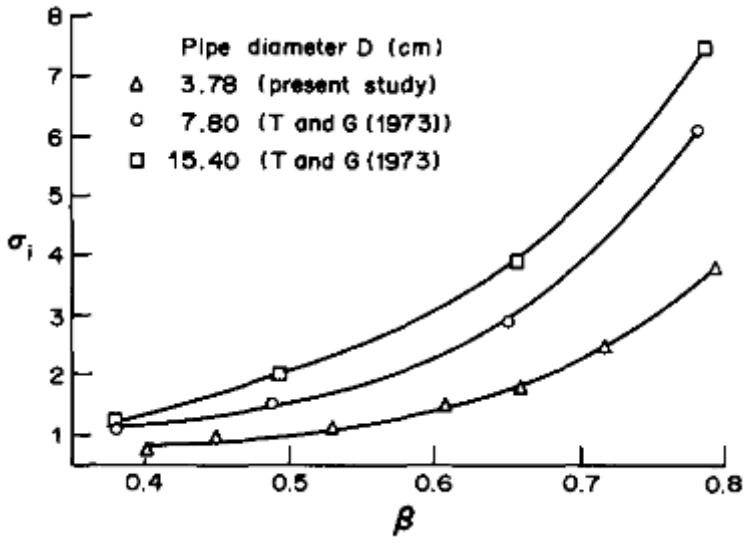

Figure 29 Comparison of experiment results from Tullis, Govindarajan and Yan

Also comparing the simulation results with those of Tullis and Yan, the increase trend of cavitation inception number as diameter ratio gets larger matches the experiments, while the overall values of cavitation inception number from simulation are smaller than experiments. This discrepancy can be explained as the water used in experiments contains large amount of air and other dissolved gas inside. This may lead cavitation easier to initiate at larger cavitation number. Another explanation to this difference is the way how experimentalists detect cavitation. They usually determine the inception of cavitation by listening to the popping noise coming out of the flow system. They don't really have to visualize the generation of bubbles to make the judgement. While in simulation, the only way to tell if cavitation is there is to actually see bubbles. The fact is noise always comes before bubbles when cavitation initiates, which makes the cavitation inception number of experiments larger than simulation.

VI.2 Steady State Study of Flow Regime Transition due to Cavitation

Cavitation is a commonly encountered phenomenon in situations where liquids are transported through pipelines. The phenomenon is essentially a combination of the release

of the dissolved gas and the vaporization of the liquid upon pressure reduction. Near inception, gas release is important, whereas at chocked and in super cavitation, the vaporization of the liquid is dominant. Therefore, the mechanism of mass transfer governs the onset and development of cavitation.

A flowing system can have different flow regimes depending on the extent of cavitation. Once cavitation occurs in a flowing system, the single liquid phase first appears as a two-phase bubbly medium in the cavitation zone. As cavitation becomes more and more severe, both the size and number of cavitation bubbles are increased. The detachment or separation of the flow from the downstream side of the orifice can be observed, a phenomenon which is called chocked cavitation. A further decrease in the downstream pressure or increase in the upstream pressure leads to super cavitation: the submerged liquid jet becomes visually apparent with the vapor and the released gas surrounding the jet. The jet contains no bubbles.

Experiments have been done by several researchers about the flow regime transition due to cavitation. Numachi et al. [11] focused his research on cavitation effects on the orifice plate discharge coefficient. He claimed that the cavitation inception number for orifice flow is independent of neither fluid velocity nor pressure, but a function of diameter ratio. Tullis and Govindarajan [20] did experiments to investigate the size scale effects on cavitation. Even though experiment method is an excellent and more straightforward way to obtain the desired results of cavitation flow, like mass flow rate and pressure field, measuring parameters like the velocity field, the volume fraction of vapor is extremely hard. Besides, once cavitation initiates, bubbles within the fluid will compromise the visibility of experiment rig, making it nearly impossible to observe where cavitation first appears.

Given all these deficiencies of the experiment study of cavitation, in this section, numerical method will be applied to find out more details of cavitation phenomenon in orifice flow. By FLUENT simulation, exact inception cavitation number and chocked cavitation number can be obtained. More information about the location cavitation occurs,

the intensity of cavitation and exact value of vapor volume fraction are all available from simulation results.

VI.2.1 Case Discription

An orifice plate with $\beta = 0.5$ in associated with a long pipe is modeled in FLUENT. Dimensions of the pipe and the orifice plate remain the same as previous discharge coefficient study. Same physical models and boundary setups are defined as those in previous section. As inlet pressure increases, cavitation number decreases, flow regime starts to transient.

VI.2.2 Results and Discussion

Five cases that can properly represent the cavitation growth process are picked up from all simulation cases shown in Table 12. These five cases correspond to the inlet pressure P_1 at 275000Pa, 385000Pa, 400000Pa, 450000Pa, 500000Pa.

Table 12 Simulatoin cases of $\beta = 0.5$

β	P_1	P_2	P_D	$P_{D/2}$	$\dot{m}$	$\sum$	Cd	Cavitation?
0.5	250000	101000	245000	72400	23.17	2.232	0.635	NO
0.5	275000	101000	268000	58500	25.57	1.899	0.636	YES
0.5	300000	101000	292000	31800	28.347	1.524	0.633	YES
0.5	350000	101000	340000	14500	31.58	1.358	0.630	YES
0.5	385000	101000	374000	3540	33.67	1.300	0.630	YES
0.5	400000	101000	388000	3540	34.37	1.291	0.631	YES
0.5	450000	101000	437000	3540	36.6	1.256	0.633	YES
0.5	500000	101000	485000	3540	38.6	1.260	0.634	YES

Figure 30 below show the vapor volume fraction of each case.

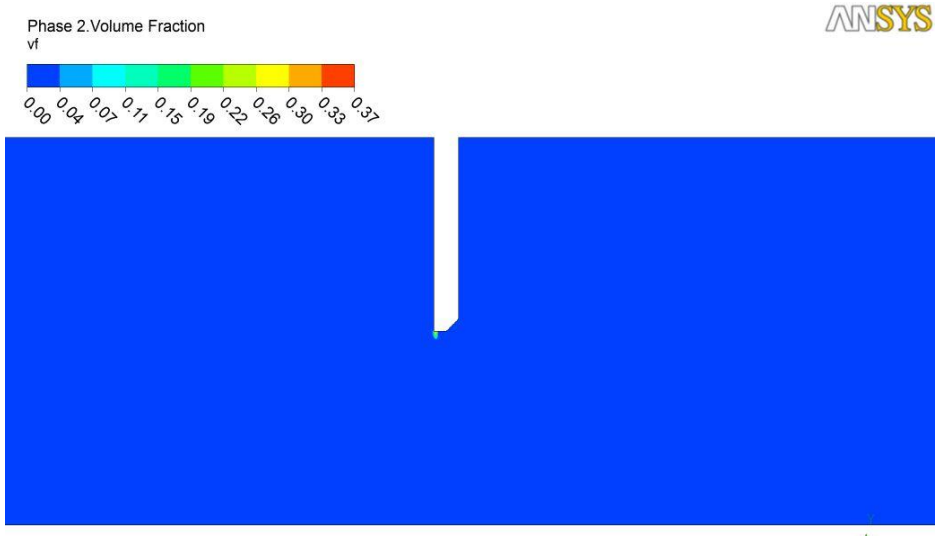

(a). β =0.5, P_1 =275000Pa, P_2 =101000Pa

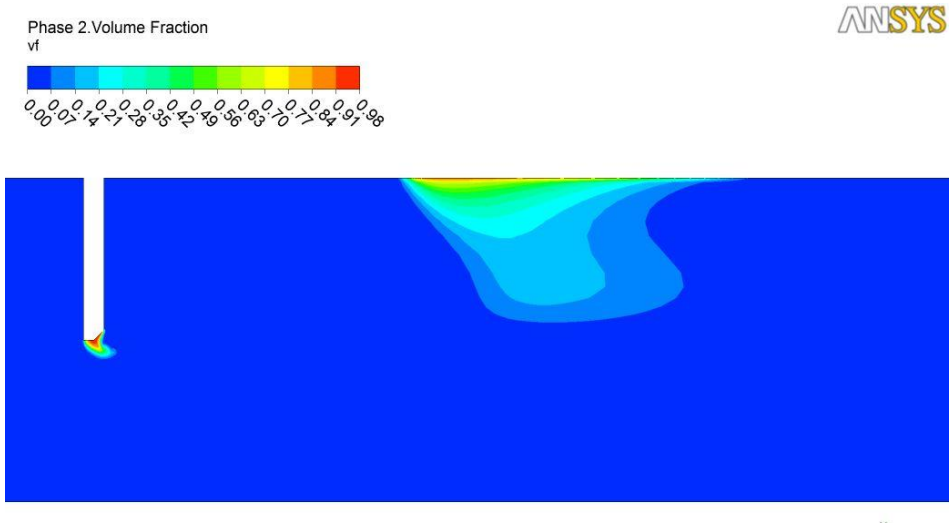

(b). β =0.5, P_1 =385000Pa, P_2 =101000Pa

Figure 30 Cavitation development as inlet pressure increases

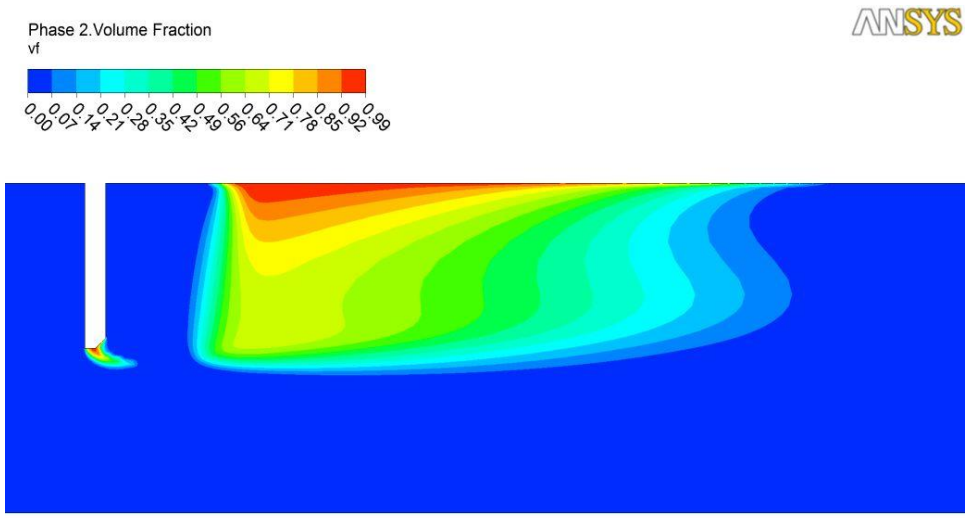

(c). β =0.5, P_1 =400000Pa, P_2 =101000Pa

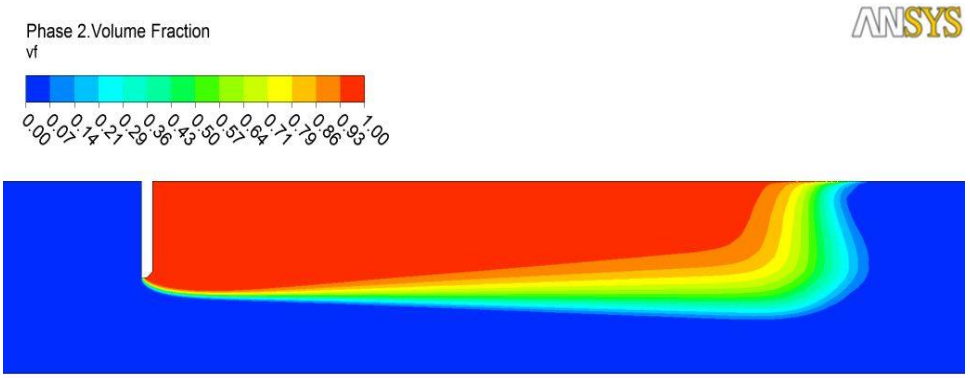

(d). β =0.5, P_1 =450000Pa, P_2 =101000Pa

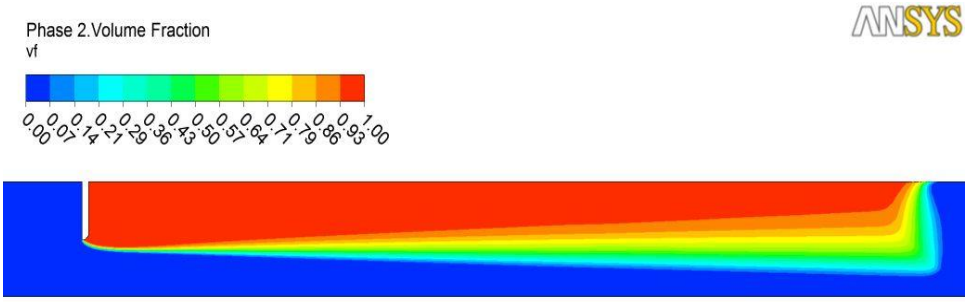

(e). β =0.5, P_1 =500000Pa, P_2 =101000Pa

Figure 30 Continued

Figure 30(a) shows the inception of cavitation. According to the definition of cavitation inception, when water bubbles first appears in flow, no matter where it is, cavitation incepts. For flow through orifice plate, thumb of rule tells us the lowest pressure will happen at vena-contracta, which is located somewhere downstream not far from the orifice centerline. This is all based on the basic Bernoulli principle. However, from the result of FLUENT simulation, cavitation didn't incept at vena-contracta. Instead, it occurred at the edge of orifice throat. The reason for this will be further exploited in the following chapter.

As inlet pressure increases, cavitation number decreases. The bubbles become more in number at orifice edge. Therefore, conclusion can be made from this phenomenon that cavitation gets stronger as cavitation number decreases. During the development of cavitation, downstream pipe wall also starts to have cavitation besides the orifice edge (see Figure 30(b)). Interestingly, these two locations where cavitation happens are not connected. At this point, it is unclear how cavitation on the downstream wall happens. Some speculations can be made:

(1). These bubbles on wall might come from the cavitation source at orifice edge. When the water flows through orifice throat, it encounters a sudden restriction and expansion. A big recirculation zone is then expected at downstream close to the wall. So bubbles generated at the orifice edge might be taken away by the water flow and end up at the recirculation core.

(2). Another speculation is that bubbles on the wall actually come from the source within themselves. For some reason, the pressure near the wall drops to the vapor pressure which causes cavitation to happen.

More evaluation about cavitation at the downstream wall will be conducted later in this paper.

What is demonstrated in Figure 30(c) is the further development of cavitation at both the orifice edge and the downstream wall. It can be noticed that the cavitation area has an obvious increase, and the volume fraction of water vapor increases as well. The region close to the wall has becomes fully vaporized with volume fraction 100%. At this critical

condition when a continuous phase of vapor near the wall happens, the cavitation is said to be chocked.

As Figure 30(d) illustrates, if the cavitation number keeps decreasing, the aforementioned two cavitation regions in pipe merge into one big continuous cavitation region. The closer to the wall, the volume fraction of vapor becomes larger till it reaches 100%. When going radically further from the wall toward the centerline of pipe, the volume fraction decreases rapidly till it becomes pure water. This stage of cavitation is called super cavitation. A schematic of this super cavitation can better describe the flow feature in terms of the phase transition (see Figure 31).

While the cavitation number continue to drop, the cavitation area will further extend downstream (see Figure 30(e)) until a phenomenon called hydraulic flip occurs.

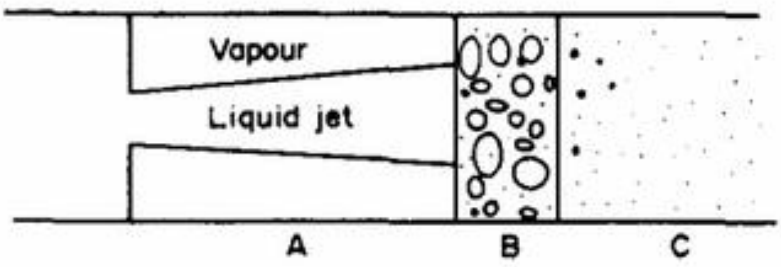

Figure 31 Flow regions at super cavitation: region A-super cavity; region B-white clouds; region C-clear liquid [17].

VI.3 Transient Study of Cavitation Inception and Development

VI.3.1 Case Description

The steady state result of $\beta = 0.5, P_1 = 400000Pa$ presented is the last section shows the vapor volume fraction contour in the flow domain (see Figure 30(c)). Then questions rise that how come two cavitation regions are totally separated. Where does the downstream cavitation come from? Therefore, in this section, a transient study of $\beta = 0.5, P_1 = 400000Pa$ is conducted primarily to explain exactly where the cavitation at downstream wall comes from. As mentioned in last section, two speculations are made for this phenomenon. First, the bubbles might be carried away from the orifice edge by the water flow. Second, a separate and independent cavitation source appears on the wall, which has nothing to do with the source at the orifice throat edge. The transient study has its own advantage of showing the dynamic feature of cavitation. The simulation covers the time ranging from 0s to 0.21s with 0.01s increment.

VI.3.2 Results and Discussion

Snapshots of vapor volume fraction contour at each time step are taken and shown below.

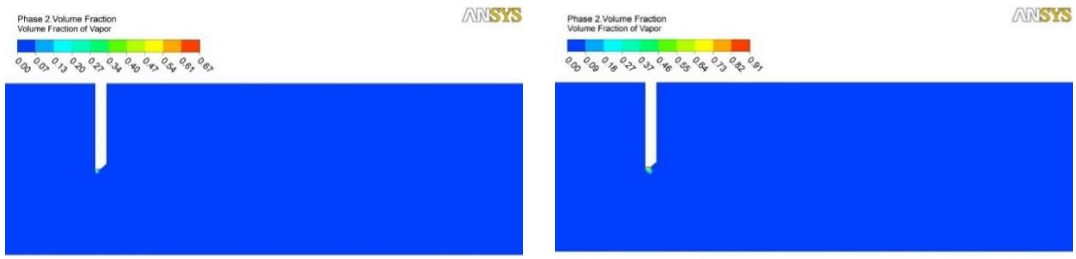

(a) 0.03s (b) 0.05s

Figure 32 Vapor volume fraction contour from 0s to 0.21s

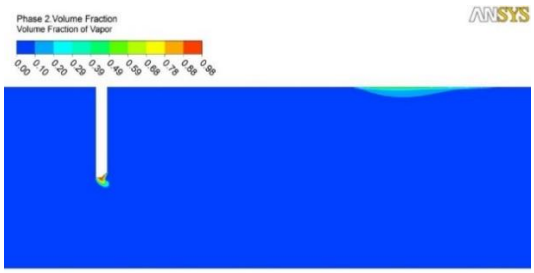

(c) 0.07s

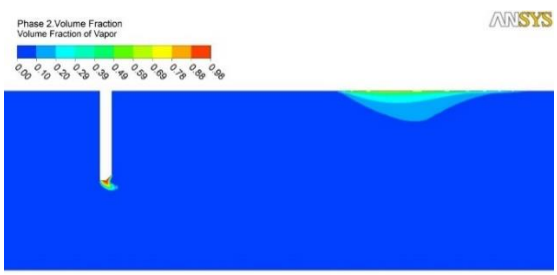

(d) 0.08s

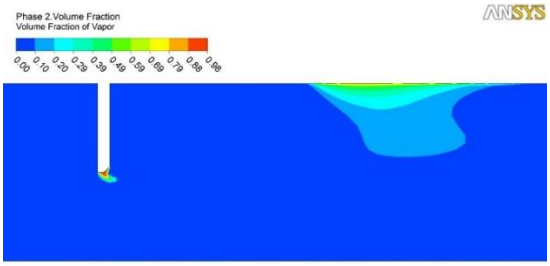

(e) 0.09s

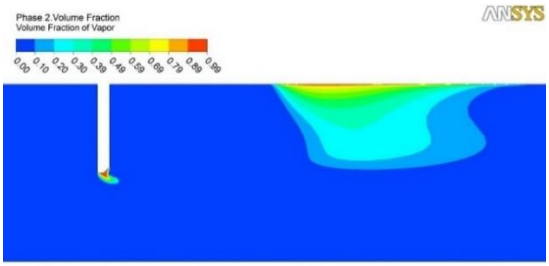

(f) 0.11s

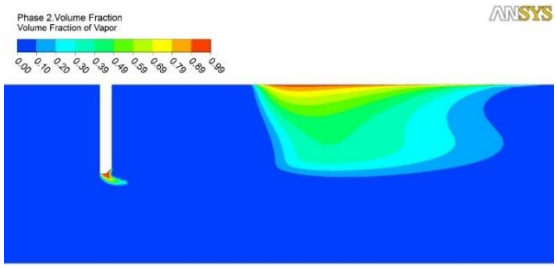

(g) 0.13s

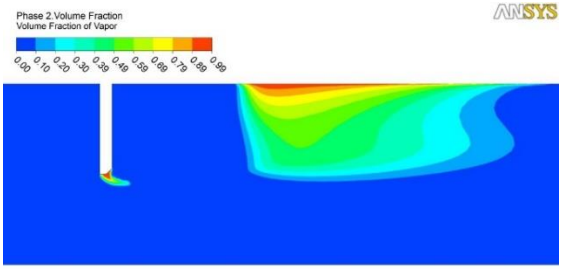

(h) 0.15

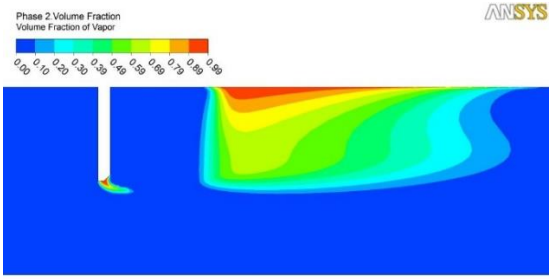

(I) 0.19s

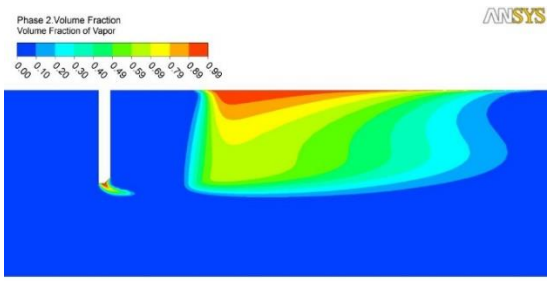

(j) 0.21s

Figure 32 Continued

From Figure 32 above, it is not hard to see the cavitation first occurs at the orifice throat edge, to be more specific, at and only at the horizontal edge. At 0.07s, the bevel edge begins to have bubbles attached on it. We can also notice at time 0.07s, the cavitation at downstream wall first appears. Before that, no sign of bubbles transporting from the orifice edge to the wall ever exist, which means a separate cavitation source shows up on pipe wall and produces bubbles. So the second speculation is right. As time goes by, both cavitation region grow gradually and tend to be steady at about 0.2s.

Besides the transient study, there is a more straightforward way to understand the two separate cavitation source. The mass transfer rate contour can be plotted based on FLUENT results (see Figure 33). The mass transfer rate represents the time rate of mass transfer between two phases (water liquid and water vapor) via cavitation. The positive value (also called source) represents the water liquid evaporating to the vapor, while the negative value (also called sink) means the vapor condenses back to the liquid.

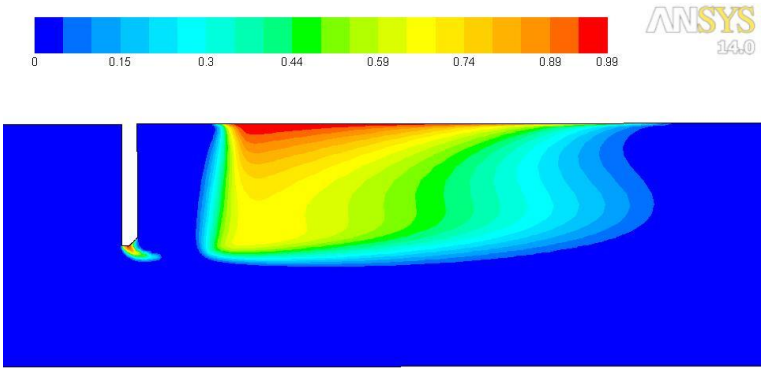

(a) Vapor volume fraction

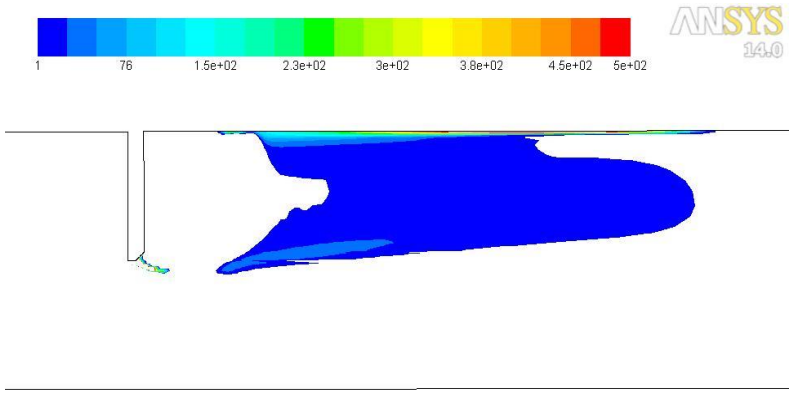

(b) Source of cavitation

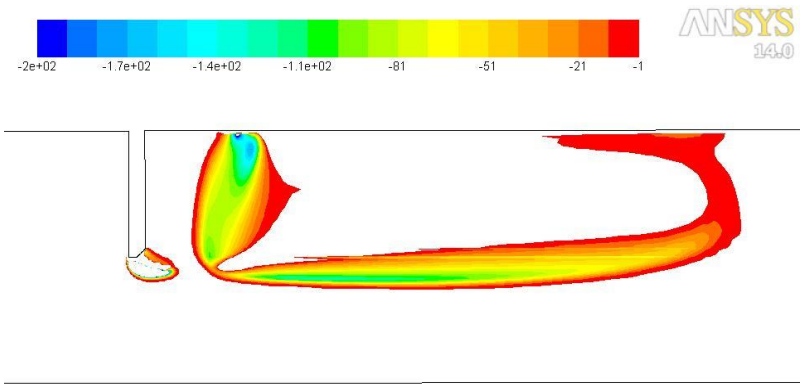

(c) Sink of cavitation

Figure 33 Mass transfer rate within the flow domain

The source of cavitation contour shows mass transfer rate ranging from 1 $kg/m^3 \cdot s$ to 500 $kg/m^3 \cdot s$. If the full spectra of the mass transfer rate is plotted, the source region at downstream wall will even out to be a uniform color since the mass transfer rate there is relatively low comparing to that at the orifice edge. Therefore, we know from the source contour that two areas have the strongest source, which are the orifice edge and the region close to the wall. As for the sink contour, the same reason clipping ranging is applied to distinguish the strong sink from the weak to get more general view of where the sink is within the flow domain. The strongest sink can be found at somewhere on the wall close to the back surface of the orifice plate.

If both source and sink contour of cavitation are overlapped based on the same scale and orifice plate position, something interesting happens. The source contour fits exactly into the slot of the sink contour. In another word, the sink completely encloses the source region. It can perfectly explain why two cavitation bubble regions are not connected. Since all bubbles evaporated from the water liquid in the source have to go through the sink region where bubbles will condense back to the water liquid, so there are no bubbles outside the sink area.

CHAPTER VII

CONCLUSION

Through the validation study, by comparing the axial velocity contour, the TKE contour, the vorticity contour as well as the velocity and pressure distributions along axis between simulation and experiment results, it is appropriate and relatively accurate to implement the k-epsilon and schnerr-sauer model to simulate the cavitation flow. Also, 3D simulation can be replaced by 2D axisymmetric simulation in favor of time and cost efficiency.

The non-dimensional study concludes that the discharge coefficient is a function of the inlet Reynold's number, the cavitation number and the diameter ratio. In associated with the simulation results in terms of cavitation effects on discharge coefficient, notice can be made that the discharge coefficient of an orifice plate is independent of both inlet Reynold's number and cavitation number. Therefore, only the diameter ratio is left out to govern the discharge coefficient if the pressure tapping method is fixed. Using the polynomial regression, a third degree correlation can be estimated with residual sum of squares 5.17×10^{-7}, shown below,

$$Cd = 0.5542 + 0.5626\beta - 1.652\beta^2 + 1.68\beta^3$$

This regression polynomial can be used to estimate the discharge coefficient at different diameter ratio.

From the plot of cavitation effects on the discharge coefficient, conclusion can also be made that the discharge coefficient value for each diameter ratio roughly matches those from Numachi's experiments. However, comparing the simulation result with those of Tullis and Yan, the increase trend of the cavitation inception number as the diameter ratio gets larger matches the experiments, while the overall values of cavitation inception number from simulation are smaller than experiments. This discrepancy can be explained as the water used in experiments contains large amount of air and other dissolved gas inside. This may lead cavitation easier to initiate at larger cavitation number.

The study of flow regime transition due to cavitation shows close dependency of flow features on the inlet pressure, in another word, on the cavitation number. As the cavitation number increases to a critical value, cavitation inception occurs at the orifice interior edge. If the cavitation number keeps increasing, water vapor bubbles start to show at the pipe downstream wall. Two speculations are made to explain the relationship between these two cavitation regions, nonetheless, the second speculation holds after the transient study, which claims bubbles on wall actually come from a source within themselves. For some reason, the pressure on the wall drops to the vapor pressure and cause cavitation to happen. The isolation of these two cavitation regions can be interpreted as that the sink completely encloses the cavitation source. Therefore, all bubbles evaporated in source have to go through the sink region where bubbles will condense back to the water liquid. So there are no bubbles outside sink area simply because no bubbles generated in the source can ever escape.

REFERENCES

[1] R. Knapp, W. Daily, F. Hammitt, *Cavitation*. McGraw - Hill, 1970

[2] W. H. Nurick, "Orifice Cavitation and Its Effect on Spray Mixing", *ASME J Fluids Eng.*, Vol. 98, pp. 681-687, 1976

[3] N. Abuaf, B. J. Wu, G. A. Zimmer, P. A. Saha, "Study of Non-equilibrium Flashing of Water in a Converging Diverging Nozzle", *office of nuclear regulatory research*, 1864

[4] R. S. Meyer, M. L. Billet, J. M, Holl, "Free Stream Nuclei and Traveling Bubble Cavitation", *ASME J Fluids Eng.*, Vol. 114, pp. 672-679, 1992

[5] B. Stutz, J.L. Rebound, "Measurements within Unsteady Cavitation", *Exp. Fluids*, Vol. 29, pp. 545-552, 2000

[6] C. M. Hansson, *ASM Handbook: Friction, Lubrication and Wear Technology*. Vol. 18, pp. 214-220, 1992

[7] C. M. Preece, "Treatise on Materials Science and Technology", *Erosion*, Vol. 16, pp. 249-308, 1979

[8] W. S. Lamb, *Cavitation and aeration in hydraulic systems. Bedfordshire*, UK. BHR Group, 1987.

[9] J. F. Bailey, "Metastable Flow of Saturated Water," *Trans. ASME*, Vol. 73, pp. 1109, 1951

[10] G. Ruppel, "Die Durchflusszahlen von Normblenden und ihreAbhangigkeit von der Kantenlange", *Zcitsehrift VDI*, vol. 80, pp. 1381, 1936

[11] F. Numachi, M. Yambe, "Cavitation effect on discharge coefficient of the sharp-edged orifice", *Journal of basic engineering*, 1960

[12] B. C. Kim, B.B. Pak, "Effects of cavitation and plate thickness on small diameter orifice meters", *Flow Measurement Instrument*, Vol. 8, No. 2, pp. 85-92, 1997

[13] S. Dabiri, D. D. Joseph, "Cavitation in an orifice flow", *Physics of Fluids*, Vol 19, pp. 72-112, 2007

[14] C.Xu, "Simulation of orifice internal flows including cavitation and turbulence", *Purdue University PHD thesis*, 2001

turbulence kinetic energy, turbulence kinetic energy production rate and correlation coefficients.

To implement similitude method, similar geometry and the same operation conditions need to be defined when conducting numerical study in FLUENT. That means, an orifice plate meter with $\beta = 0.5$ and $\beta = 0.75$ should be modeled and meshed. In addition, the inlet Reynolds number have to be exactly identical with those in experiments. So two cases are chosen for this validation study, which are $\beta = 0.75$, $\mathrm{Re} = 54700$ and $\beta = 0.5$, $\mathrm{Re} = 91100$. Both cases have fixed pressure at outlet of pipe, as much as 1 atm. The geometry and boundary condition setup in FLUENT are shown in Figure 9.

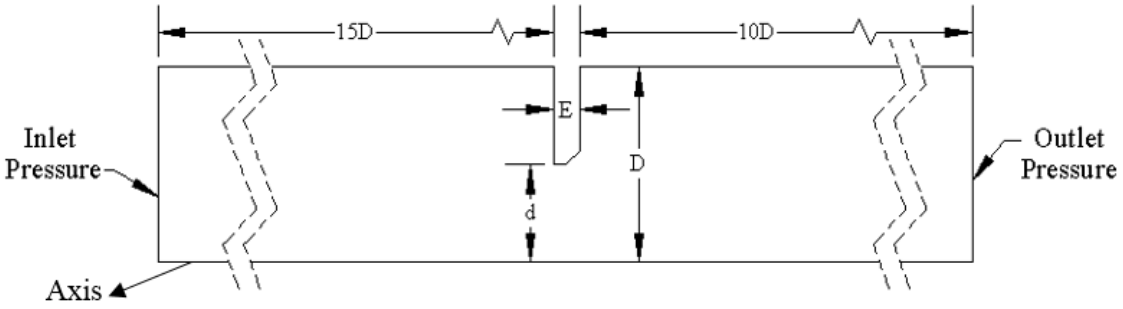

Figure 9 Geometry and boundary condition setup

Regarding the fact that the flow domain within pipe is going to be axisymmetric, it is not necessary to do the whole domain simulation. As a result, only half of a cross-section area is chosen to be the flow domain for purpose of calculation efficiency. To verify the accuracy of the 2D axisymmetric simulation, more details about 3D simulation and 2D axisymmetric simulation comparison will be discussed later.

The mesh is generated by GAMBIT and imported in FLUENT (shown in Figure 10). Only the critical mesh region, the orifice plate region, is shown in the figure due to the excessive length of the pipe. The mesh at orifice throat is densified since there occurs significant pressure and velocity gradient and it might also be the place where cavitation appears. The boundary layers of the flow near the walls also desire finer mesh.